Geodynamics along an increasingly curved convergent plate boundary: Late Miocene-Pleistocene Rhodoes, Greece

ten Veen, J.H.; Kleinspehn, K.L.

published in
Tectonics
2002

DOI (link to publisher)
10.1029/2001TC001287

document version
Publisher's PDF, also known as Version of record

Geodynamics along an increasingly curved convergent plate margin: Late Miocene-Pleistocene Rhodes, Greece

Johan H. ten Veen[1] and Karen L. Kleinspehn

Department of Geology and Geophysics, University of Minnesota, Minneapolis, USA

Received 23 February 2001; revised 31 October 2001; accepted 16 December 2001; published 19 June 2002.

[1] Neogene-Holocene outward migration of the absolute position of the convergent Hellenic plate boundary produced simultaneous increased curvature of the plate boundary, changing obliquity of plate convergence vectors and boundary-parallel stretching of the forearc region. To study the effects of the plate boundary migration and curvature, a tectonostratigraphy is constructed from the middle Miocene–Pleistocene Apolakkia basin on Rhodes, whose easternmost location makes it a key island to assess the inner forearc's kinematic response to expansion of the overriding Aegean-Anatolian block and thus obliquity of convergence with the African plate. The basin fill provides temporal and paleogeographic control to interpret its syndepositional and postdepositional structural assemblages. Five fault populations in the Apolakkia basin record two neotectonic deformation phases separated by a kinematic change at ~4.5 Ma, both of which are consistent with outward expansion of the Aegean-Anatolian block. The Apolakkia basin originated as a late Miocene fault wedge basin in response to syndepositional southwest-northeast D1 extension with similar strain patterns in the adjacent offshore Hellenic inner forearc. The kinematic change at ~4–5 Ma is attributed to a threshold of obliquity whereby the inner forearc started to experience sinistral-oblique divergence. The Plio-Pleistocene D2 transtensional phase reoriented the basin and resulted in combined syndepositional west-northwest-east-southeast ex-tension (283°) and 070° sinistral shear, orientations that are best attributed to simultaneous outward expansion of the Hellenic forearc, increasing curvature of the plate boundary and associated boundary-parallel stretching of the forearc. Principal shear zones offshore also occur consistently at ~070°, mimicking the D2 kinematic history of the Apolakkia basin and suggesting a consistent geodynamic regime throughout the inner eastern Hellenic forearc. Effects of sinistral-oblique plate convergence along the subduction zone appear confined to the outer forearc and the accretionary prism of the Mediterranean Ridge. Thus the upper crust of the expanding Aegean-Anatolian block behaved independently at its leading edge, and the Pliny "trench" constitutes a major boundary separating partitioned forearc slivers, a post-4.5 Ma partitioning recorded reliably by the Pliocene fill of the Apolakkia basin. *INDEX TERMS:* 8150 Tectonophysics: Evolution of the Earth: Plate boundary—general (3040); 8105 Tectonophysics: Continental margins and sedimentary basins; 8107 Tectonophysics: Continental neotectonics; 9335 Information Related to Geographic Region: Europe; 8015 Structural Geology: Local crustal structure; *KEYWORDS:* oblique plate convergence; neotectonics; Greece; transtension; forearc basin; oblique divergence.

1. Introduction

[2] Gradients in plate convergence obliquity along a curved subduction zone produce arc-parallel gradients in the horizontal shear stress with resultant deformation of forearcs [*McCaffrey*, 1996]. At some point along a strongly curved subduction zone, the plate motion vectors may become subparallel to the plate boundary, and relative motion between the plates is essentially subhorizontal along the inclined interface between the two plates. Although the kinematics along obliquely convergent plate boundaries have been addressed elsewhere, including the Aleutian volcanic arc [e.g., *Geist et al.*, 1988; *Avé Lallemant and Oldow*, 2000], the Sunda arc [*McCaffrey*, 1988], the Leeward Antilles arc [*Avé Lallemant and Guth*, 1990], and the forearc of the Hikurangi subduction zone [*Cashman et al.*, 1992; *Chanier et al.*, 1999], the Hellenic plate boundary, Greece, has the added attraction that its curvature and consequent obliquity of convergence has increased systematically since middle-late Miocene time (11 Ma; Figure 1).

[3] Increased curvature of the Hellenic plate boundary has been attributed to several individual or combined processes including the following (1) rollback of the subduction interface induced by pull of the downgoing African slab [*Le Pichon and Angelier*, 1979; *Le Pichon*, 1982; *Meulenkamp et al.*, 1988], (2) gravitational body forces associated with overthickened Alpine crust [e.g., *Le Pichon et al.*, 1995; *Jolivet*, 2001], (3) the westward extrusion of the Anatolian block along the North Anatolian fault [*Taymaz et al.*, 1991; *Le Pichon et al.*, 1995], and (4) Oligocene-Quaternary back arc spreading in the northern Aegean Sea (Figure 2a) [*Le Pichon*, 1982; *Gautier and Brun*, 1994]. Regardless of the driving mechanism, the plate boundary

[1]Now at Department of Earth and Life Sciences, Free University, Amsterdam, Netherlands.

0278-7407/02/2001TC001287$12.00

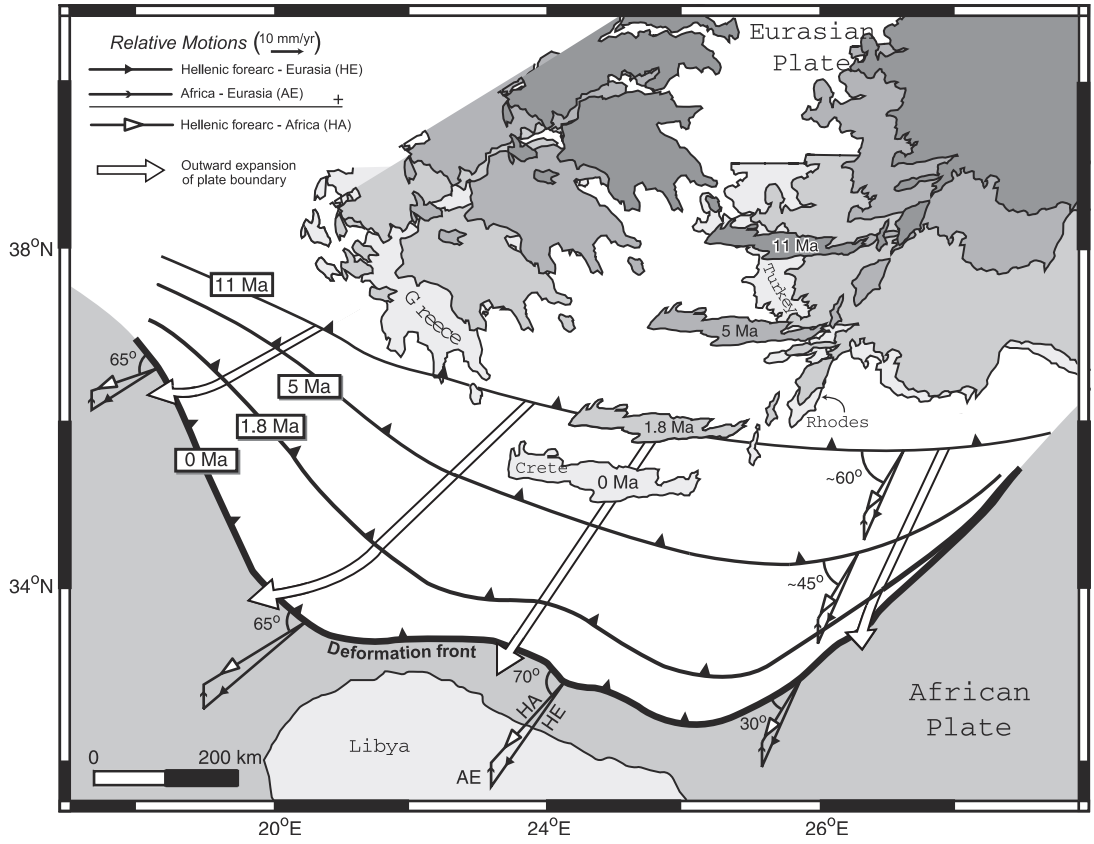

Figure 1. Increasing arc curvature and changing angle of plate convergence along the Hellenic forearc since 11 Ma (late Miocene) together with reconstructed paleogeography of the Aegean region using a Mercator projection of modern coastlines. This reconstruction is modified from *Angelier et al.* [1982] using geodetic data [*McClusky et al.*, 2000] and paleomagnetic rotation data [*Duermeijer et al.*, 2000] for estimates of the outward migration of the Hellenic forearc relative to Eurasia (HE) since 11 Ma. Africa–Eurasia motion (AE) is assumed constant since Oligocene time [*Besse and Courtillot*, 1991]. Decreasing angle of plate convergence since 11 Ma is based on the Hellenic forearc–Africa vectors (HA), which are the vector sums of AE and HE, along the increasingly curved subduction zone.

has stepped southward (Figure 1) but remained fixed at its western (Kephalonia fault) and eastern extremities (SW Turkey), forcing plate convergence vectors to evolve with changes most strongly expressed along the easternmost and westernmost Hellenic subduction zone. Polar wander data from both the Eurasian and African plates suggest no significant changes in their vectors since Oligocene time [*Besse and Courtillot*, 1991], making the obliquity of convergence at the plate boundary the product of changing plate boundary curvature.

[4] Convergence between the African plate and the Hellenic forearc is nearly perpendicular along western Crete and highly oblique (30°) in the eastern Hellenic forearc along Rhodes (Figure 1). Between Crete and the Mediterranean Ridge, en echelon segmented, bathymetric troughs, originally called the Hellenic ''trenches'' because they were thought to be the subduction zone, demarcate subparallel sinistral strike-slip zones within the forearc (Figure 2a) [*Jongsma*, 1977; *Le Pichon et al.*, 1979; *Huchon et al.*, 1982; *Peters and Huson*, 1985]. Authors *ten Veen and Meijer* [1998] proposed a latest Miocene threshold at which the plate boundary became sufficiently arcuate to force the forearc to partition into oblique slip and strike slip with a change in Pliocene strain trajectories also noted by *Angelier et al.* [1982]. Although sinistral wrench tectonics have been indicated by paleomagnetic data from Pliocene basins on forearc islands [*Duermeijer et al.*, 1998; *Duermeijer et al.*, 2000], no onshore structural studies corroborate the onset and/or persistence of sinistral wrench tectonics in the Hellenic forearc.

[5] To study the effects of the plate boundary migration and curvature, we construct a tectonostratigraphy from the Neogene-Pleistocene Apolakkia basin on Rhodes, whose easternmost location makes it a key island to assess the forearc's kinematic response to expansion of the Aegean-Anatolia block, and thus obliquity of convergence, through time. We focus on a sedimentary basin with initially subhorizontal strain markers because its chronostratigraphy constrains the timing of deformation, and we present a new interpretation of the neotectonics of Rhodes and the

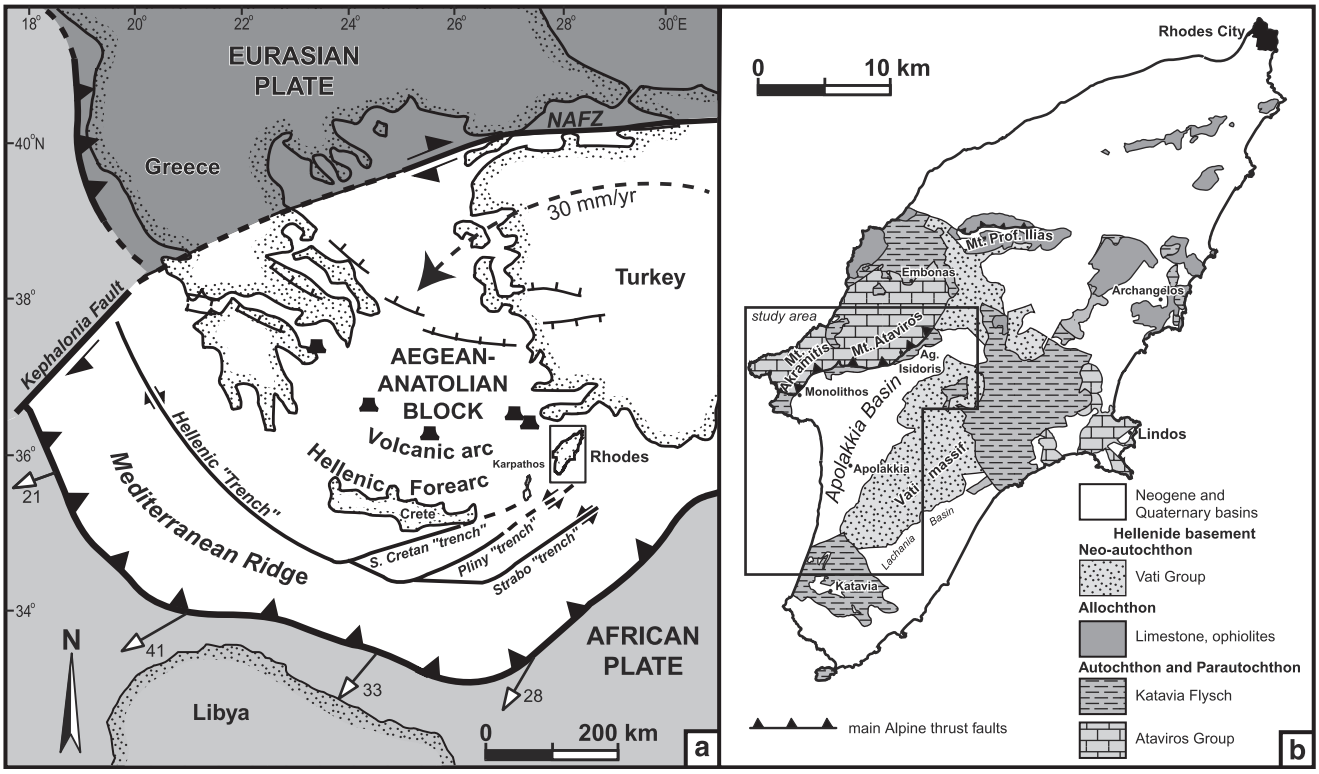

Figure 2. (a) Simplified tectonic map of the eastern Mediterranean area. The Hellenic subduction zone is shown as a heavy toothed line between the African plate (light shading) and the overriding Aegean-Anatolian block (no shading), which is associated with the Eurasian plate (dark shading). Arrows along the southern margin of the Aegean-Anatolian block denote the vectors of south-southwestward relative motion (mm/yr) between the Hellenic forearc and Africa (HA in Figure 1). The Aegean lithosphere expands over the subducted oceanic lithosphere between the Kephalonia fault and SW Turkey, which are assumed fixed points [*Meijer and Wortel*, 1997]. Dashed line indicates the westward extrusion of the Aegean-Anatolian block along the North Anatolian Fault Zone (NAFZ) relative to a fixed Eurasian plate [*Le Pichon et al.*, 1995]. Inset shows location of Figure 2b. (b) Simplified geological map of Rhodes, showing the distribution of basement units and Neogene-Quaternary basins (modified after *Mutti et al.* [1970]). Inset shows the studied Apolakkia basin of Figure 5.

eastern Hellenic forearc using comprehensive structural data from this basin.

2. Geological Framework

[6] The island of Rhodes (Greece) represents an uplifted segment of the Hellenic forearc. Middle Miocene-Pleistocene sedimentary basins, including the Apolakkia basin, are separated by a stack of Alpine nappes of the Hellenide-Tauride orogen exposed in uplifted fault blocks (Figure 2b). Significant Oligocene-lower Miocene unroofing of the nappe stack generated the marine molasse-flysch of the Vati Group (Figure 2b). Later Miocene emergence of the island with absence or removal of Miocene deposits recorded late Alpine folding [*Mutti et al.*, 1970].

[7] Mio-Pliocene normal faulting generated restricted continental basins filled by coarse-grained sediments [*Bukowski*, 1899]. The first of four phases in the Miocene-Pleistocene basin fill involved mainly Miocene to early Pliocene erosion of the basement units [*Meulenkamp et al.* 1972]. During the second phase, an early late Pliocene fluvio-lacustrine island-wide basin accommodated a large sediment flux from the east and northeast. In the Apolakkia basin the early Pliocene age of this phase (middle-late Ruscinian) is based on mammal assemblages from the Istrios and Apolakkia Formations [*Benda et al.*, 1977; *van de Weerd et al.*, 1982; *Kovacs and Spjeldnaes*, 1999], an age that constrains the timing of syndepositional deformation. During the third phase a late Pliocene marine transgression along the north and east coasts marked a general eastward tilt that is still apparent in the modern island. The Apolakkia area was simultaneously block faulted, isolating the basin from the rest of Rhodes, and lacustrine conditions were recorded in the northern part of the basin as limestone (travertine) of the Monolithos Formation (Figure 3) [*Meulenkamp et al.*, 1972]. An upper Pliocene caliche largely of pedogenic origin, the "Poros," then developed throughout the Apolakkia basin (Figure 3) [*Mutti et al.*, 1970]. In Pleistocene phase 4, the island became separated from mainland Turkey. Terraced regressive cyclic marine sequences along the present eastern Rhodes coast

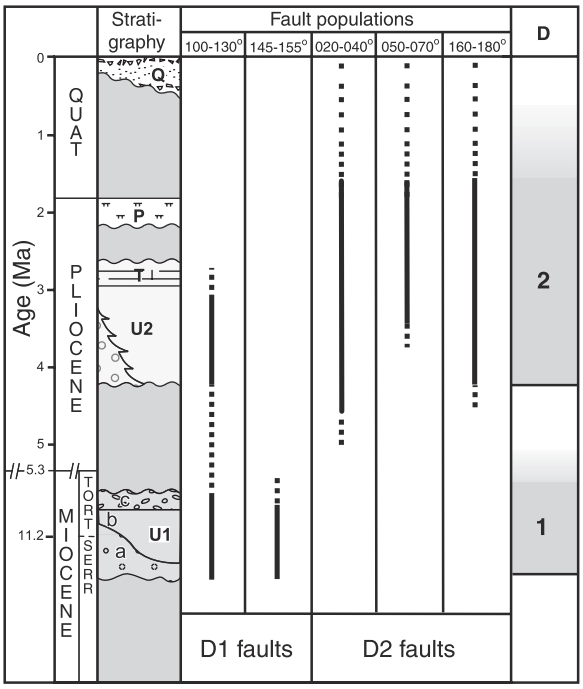

Figure 3. Simplified middle Miocene-Quaternary tectonostratigraphy of the Apolakkia basin with absolute ages for Pliocene and younger strata from *van Vugt* [2000]. Labels are as follows: U1, Unit 1 (including subunits a, b, and c); U2, Unit 2, including travertine (T); P, pedogenic Poros Formation; and Q, Quaternary alluvium. See text and Figure 5 for explanation of patterned lithofacies. For each fault population, inferred fault activity is represented by dashed lines but is represented by solid lines when activity is certain, yielding two deformation phases, D1 and D2.

were attributed to differential vertical tectonic movements [*Meulenkamp et al.*, 1972; *Hanken et al.*, 1996; *Hansen*, 1999]. Ongoing dissection of the Poros surface is governed by active tectonism.

[8] *Duranti* [1997] revised the Pliocene stratigraphy of the Apolakkia basin, and his Unit 1, which we adopt (Figure 3), consists of $\geq$300 m of mixed fan delta, fluviolacustrine, and alluvial fan facies deposited predominantly along the southeastern basin margin. On the basis of freshwater gastropods, *Willmann* [1980] assigned a middle-late Miocene age (Serravallian/Tortonian) to the basin fill resembling Unit 1 (Figure 3).

[9] Within the $\geq$700-m-thick Unit 2, *Duranti* [1997] recognized 40–100-m-thick sequences starting with a lacustrine delta-plain association overlain by a palustrine association and followed by a shallow lacustrine association consisting of alternating lacustrine marl and pedogenic carbonates (paleosols), lignite, and sand sheets. In the northwestern Apolakkia basin, this upper facies association also contains lacustrine travertine (Figure 3). *Duranti* [1997] attributed the cyclic sequences to lake-level changes of climatic origin. Subsequently, *van Vugt* [2000] examined potential control by astronomical cycles and climate and reinforced a mid-Pliocene age for Unit 2 by correlating the basin's magnetostratigraphy with the polarity timescale of *Lourens et al.* [1996]. In contrast, we examine the basin's structural geology to assess a potential role of tectonics in controlling basin evolution and facies architecture.

3. Structure and Tectonosedimentary Development of the Apolakkia Basin

[10] The Pliocene-Pleistocene tectonosedimentary development of the Apolakkia basin can be attributed to deformation along four populations of basin-scale lineaments identified initially on Landsat satellite images (Figure 4). In the field, the large lineaments correspond to four populations of observed master faults. However, many lineaments ($\sim$80%) were not recognizable in the field, but they parallel major fault zones and are likely related to structural phenomena. A fifth fault population identified in the field comprises outcrop-scale faults with only limited expression in the satellite imagery. On the basis of the ages and sequence of fault activity, two deformation phases (D1 and D2) are recognized for the Neogene-Pleistocene Apolakkia basin (Table 1; Figures 3 and 5).

[11] We determined the sense of shear along faults using sigmoidal gouge fabric, orientation of drag folds, and offset stratigraphic markers. We also relied on slickensides and groove marks on the fault planes to interpret the sense of shear [*Petit*, 1987]. We regard faults as normal faults if the pitch of the slip indicator or rake (r) is $80° \leq r \leq 90°$ (pure dip slip), as oblique-slip faults if $10° < r < 80°$, and as strike-slip faults if $r \leq 10°$. Faults recording oblique slip dominated by the dip-slip component are called normal-sinistral faults, whereas sinistral-normal faults were dominated by the strike-slip component.

3.1. 100°–130° Basin-Scale Oblique-Slip Faults

[12] South dipping dextral-oblique, dextral-normal, and normal-dextral faults dominate the 100°–130° fault population, whereas north dipping faults and/or sinistral-normal faults are less abundant (Table 1). Although these faults parallel the strike of basement thrusts (Figure 5), their dips are subvertical. Many similarly trending lineaments appear to transect the basin in the satellite images on which they display a narrower spread in orientation (Figure 4) compared to the mapped faults (Figure 5).

[13] Along the southeast basin margin where these faults are better expressed, variations in Unit 1B thicknesses on fault blocks along the subvertical Profilia fault zone (PFZ) (Figure 5) suggest that faulting started during the late Miocene deposition of Unit 1 [*Duranti*, 1997]. The magnitude of dip-slip offset of Unit 1 stratigraphic markers diminishes upward suggesting syndepositional subsidence of the fault block south of the PFZ. Clast imbrication in channel-fill conglomerates records sediment sources to the north-northeast [*Duranti*, 1997], suggesting derivation from the uplifted block.

[14] Although the principal fault activity occurred in late Miocene Unit-1 time, a few 100°–130° faults record middle-late Pliocene D2 reactivation in the form of amphitheatrical folds, sigmoidal shear fabrics, and slickenlines in

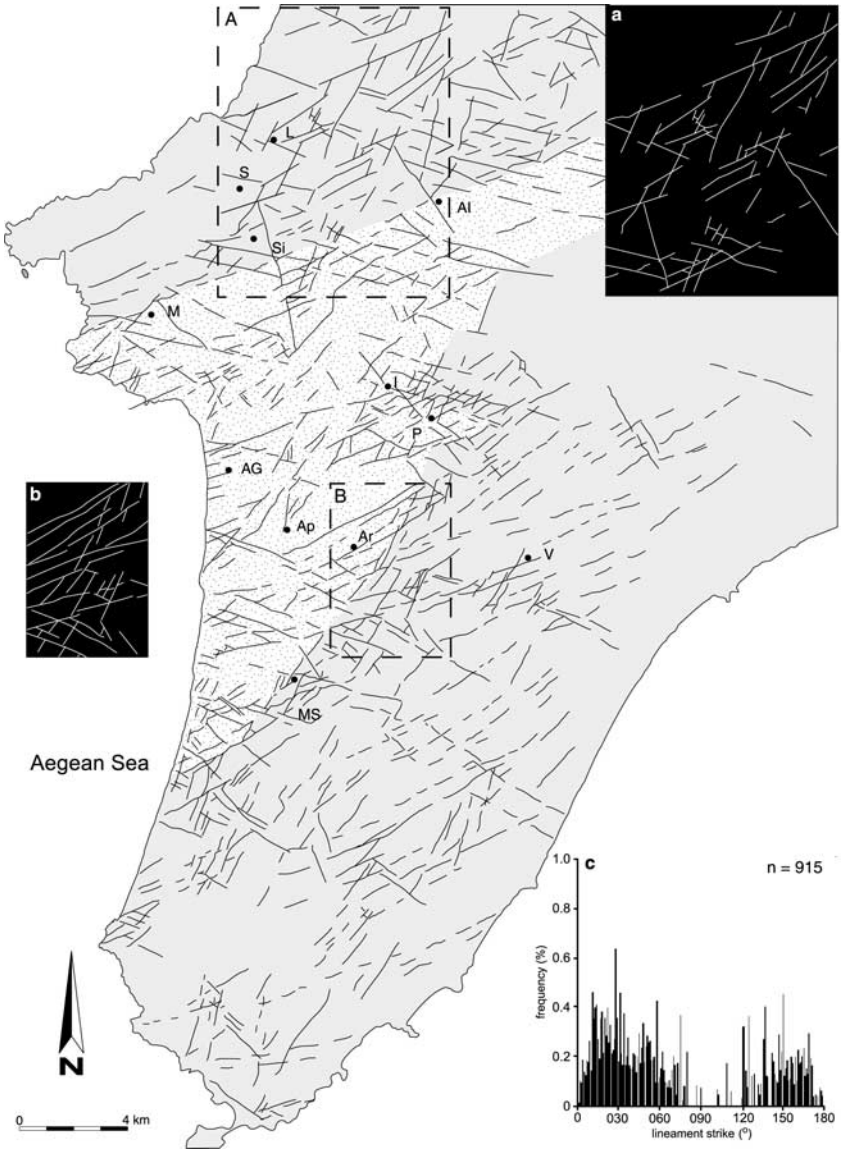

Figure 4. Lineament interpretation of Landsat TM5 satellite imagery for southern Rhodes with the stippled Apolakkia basin of Figure 5. (a) Highlight of the offset of 030° lineaments by 070° lineaments and offset of 120° lineaments by 030° lineaments. (b) Highlight of the relationship between 050° and 070° lineaments as well as crosscutting 030° lineaments. (c) Histogram of strikes versus weighted frequency of 915 lineaments from Figure 4. Abbreviated localities correspond to Figure 5.

Unit 2 (Table 1). None of the observed faults of the 100°–130° population appeared to cut the upper Pliocene Poros or Quaternary deposits. Unit 2 cover precludes a detailed reconstruction of the basin geometry, but the 100°–130° fault population clearly influenced Unit 1 sedimentation, and its faults likely served as basin-bounding faults.

3.2. 145°–155° Basin-Scale Faults

[15] Exposures of the 145°–155° faults are restricted to the basin's margins and basement. Reliable slip indicators for the 145°–155° faults were consistently absent although the faults were clearly mappable; thus interpretation of the sense of slip relies on map patterns and dips of the Vati Group and upper Miocene Unit 1 that suggest the faults experienced dominantly normal slip. Locally the magnitudes of dip-slip displacement diminish upward within Unit 1, indicating syndepositional fault activity in late Miocene time. No faults of this group were found to affect the Pliocene Apolakkia basin fill, suggesting that these faults were pre-Pliocene.

[16] The 145°–155° population was presumably active concurrently with the 100°–130° fault population, whose age is also late Miocene, and is therefore assigned to a D1 deformation phase (Figure 3). That a 155° fault displaced a 120° fault, despite the 100°–130° faults being longer lived, suggests a likely conjugate relation between the two coeval fault populations during initiation of the basin. Unit 1

Table 1. Summary of Field Observations of Basin-Scale Faults of the Apolakkia Basin That Provide the Basis for Kinematic Interpretation and Deformation Phases D1 and D2[a]

Site	Fault Strike	Fault Dip	Slip Indicator	Rake	Sense of Slip	Downthrown Block
			Deformation Phase D1			
100°–130°						
Agh. Pandaleimonos	125°	80°S	slickenlines	75°NW	dominant normal dextral	south
SW of Monolithos	129°	84°S	slickenlines, sigmoids	50°NW	dextral oblique	south
PFZ	125°	80°S	sigmoids	–	sinistral	south
500 m south of PFZ	120°	90°	strike-slip component from map pattern	–	dextral	north
2 km south of PFZ	120°	subvertical	–		dextral oblique	south
East of Agh. Isidoris	127°	75°S	slickenlines	70°SE	normal sinistral	south
East of Agh. Isidoris	120°	subvertical	strike-slip component from map pattern	–	dextral oblique	north
East of Agh. Isidoris	105°	84°N	slickenlines	01°–90°E	dominant dextral oblique	north
North of Mt. Aspropetres	124°	71°N	slickenlines, sigmoids	06°NW	sinistral	north
145°–155°						
Istrios-Laerma	155°	~80°N	map pattern and stratigraphic thickness	–	dominant dip slip	north
			Deformation Phase D2			
020°–040°						
SFZ east	025°	67°W	sigmoids, drag folds, and slickenlines	–	dip slip	west
SFZ west	030°	80°E	groove marks	70°NE–79°SW	~dip slip	east
050°–070°						
MAIFZ, west of Monolithos	060°	subvertical	sigmoids and offset stratigraphy	–	dominant dip slip	south
SW of Monolithos	073°	74°S	groove marks and displaced clasts	28°N	sinistral normal	south
MAIFZ, south of Siana	070°	subvertical	sigmoids	–	sinistral oblique	south
AFZ	065°	subvertical	shear fabric, slickenlines	35°SW	sinistral oblique	north
SE Profilia	070°	subvertical	displaced clasts	–	sinistral oblique	south
NE Profilia	070°	subvertical negative flower structure	–	–	presumed strike-slip component	?
SE Arnitha	060°	subvertical negative flower structure	displaced clasts	–	sinistral oblique	north
160°–180°						
SE Monolithos	174°	80°E	slickenlines, drag folds, sigmoids	50°S	normal dextral	east

[a]Locations are shown in Figures 5 and 6. Abbreviations are as follows: PFZ, Profilia fault zone; SFZ, Siana fault zone; MAIFZ, Monolithos-Aghios Isidoris fault zone.

thicknesses observed in the eastern basin suggest a fault wedge horst with adjacent depocenters to both the north and south. Thus the Apolakkia basin likely originated as a series of fault wedge subbasins oriented approximately perpendicular to the modern basin exposure but formed under northeast-southwest extension.

[17] In the satellite images, the basin-scale 155° lineaments appear to terminate against 030° and 070° lineaments, whereas the 120° lineaments are clearly displaced by 030° lineaments (Figure 4). Such relations were corroborated in the field, which together with stratigraphic limits on the timing of fault activity give rise to a second tectonostratigraphic phase, D2.

3.3. 020°–040° Basin-Scale Normal Faults

[18] Major faults of the 020°–040° group, especially evident in the northern basement, represent normal faults,

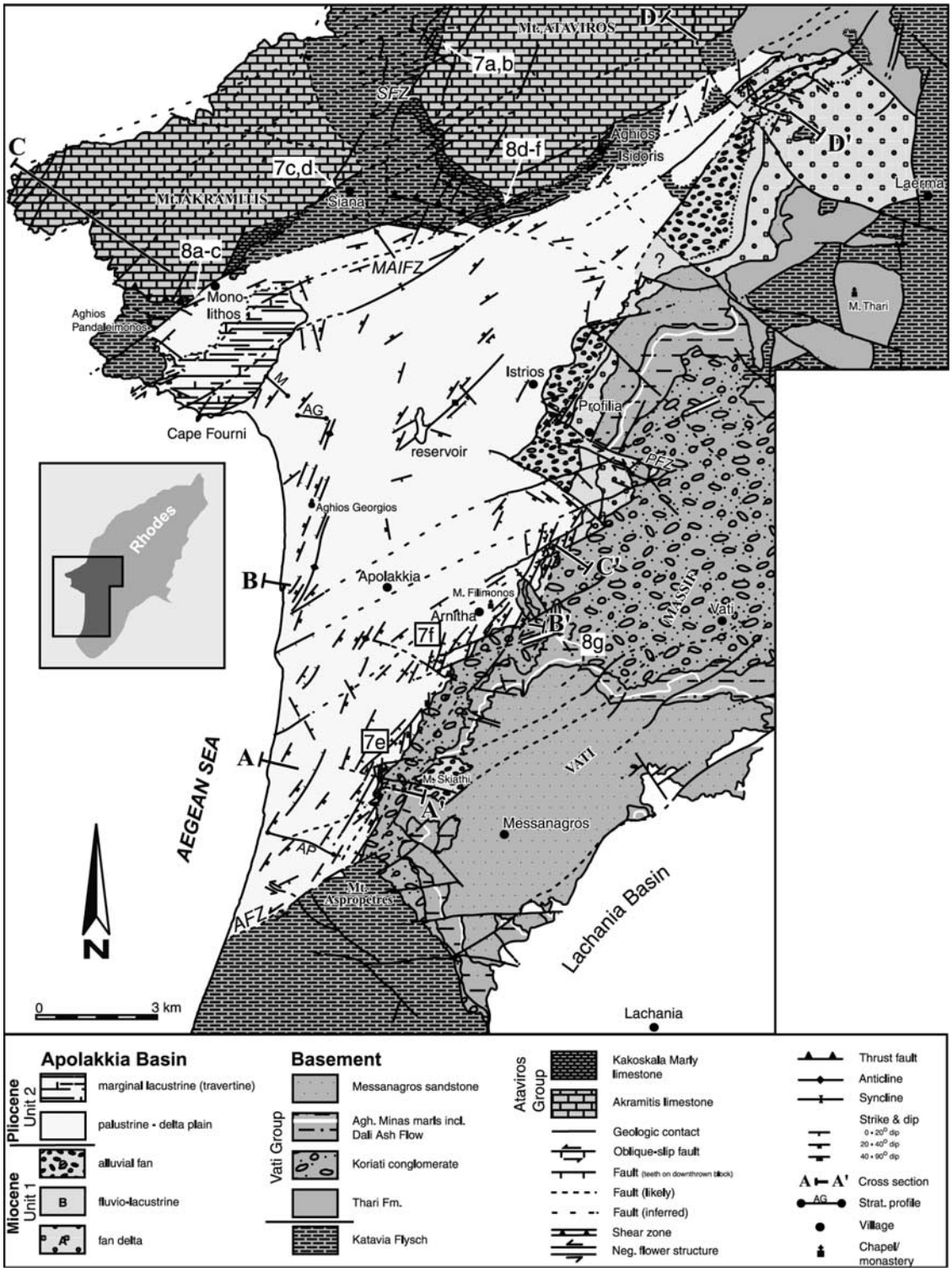

Figure 5. Geological map of the Apolakkia basin. Cross sections A–A′ to D–D′ are shown in Figure 6. Basement geology is adapted from *Mutti et al.* [1970]. Abbreviations are as follows: MAIFZ, Monolithos–Aghios Isidoris fault zone; SFZ, Siana fault zone; PFZ, Profilia fault zone; AFZ, Aspropetres fault zone. Numbers in white boxes denote locations for Figures 7 and 8.

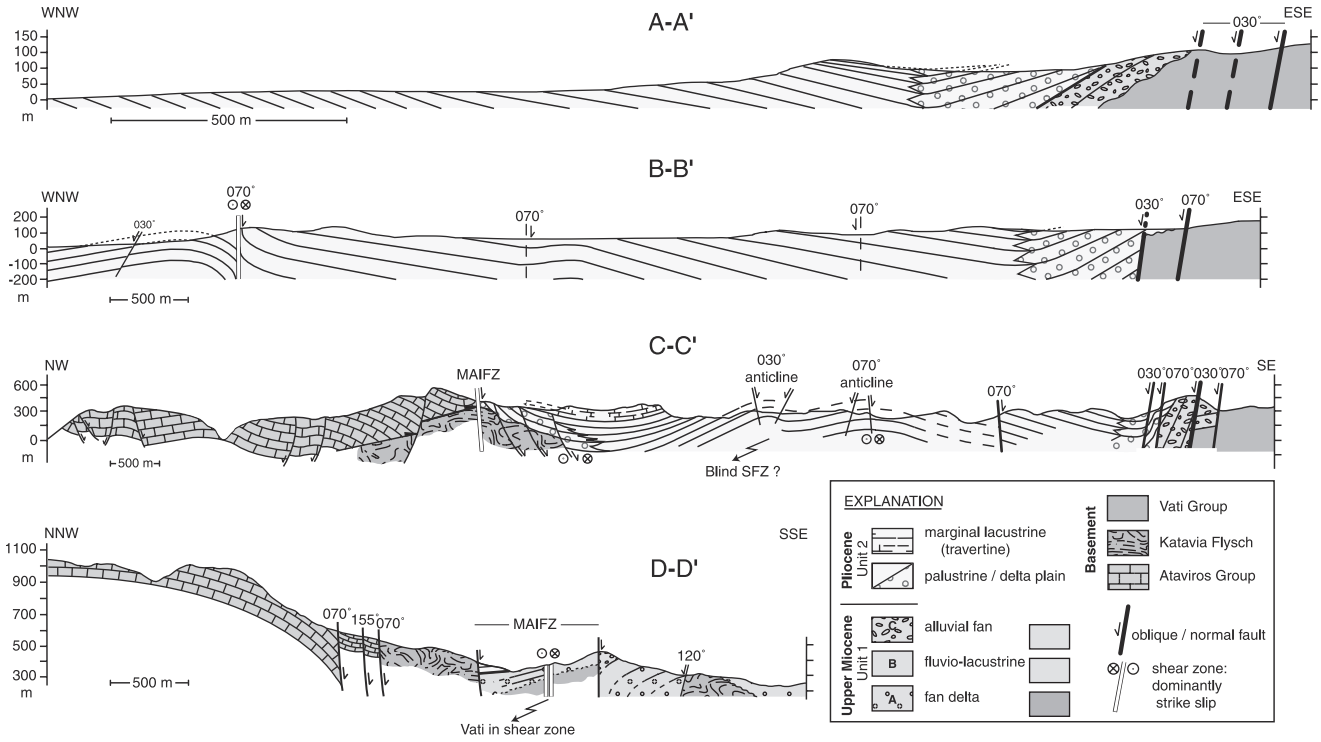

Figure 6. Cross sections through the Apolakkia basin showing the basin-scale faults (indicated by their strikes in degrees) and effects of syndepositional deformation. See Figure 5 for locations. Structural relationships at depth are speculative but inferred from mapped relations and consistent structural trends.

whereas only few, outcrop-scale faults had normal-dextral or normal-sinistral slip (Table 1). For example, subparallel 030° faults delineate a graben (Siana fault zone (SFZ); Figures 5 and 6) whose west dipping eastern fault shows a considerable vertical offset (>100 m) based on the juxtaposition of two basement limestones that stratigraphically overlie each other on the uplifted block to the east. A 30-m-wide anticlinal drag fold (Figure 7a) and sigmoidal deformation indicate nearly pure dip slip (Figure 7b). At the base of the basement massif, a subvertical fault plane is exposed over a distance of several hundreds of meters (Figure 7c), along which the limestones on the southern fault block were displaced vertically at least the height of the 70-m fault plane. The entire fault plane displays subvertical groove marks, and locally fault breccias adhere to the fault plane (Figure 7d). Constraints on the inception of the SFZ are unavailable, although satellite imagery (Figure 4, inset "a") shows that some 120° lineaments are displaced by 030° lineaments indicating that 020°–040° faulting likely postdated the late Miocene onset of 100°–130° fault activity. Unit 2 displays several signs of associated deformation:

1. Asymmetric synclines display stratal onlap and older strata dip more steeply attesting to progressive folding during deposition (cross sections AA′ and BB′; Figures 6 and 7f). These fanning dips resemble those in studies of syndepositional folding [*Hardy and Poblet*, 1994; *Burbank et al.*, 1996; *Gawthorpe et al.*, 1997; *Gupta et al.*, 1999].

2. An angular unconformity of $\leq$30° is observed (cross sections AA′ and CC′; Figures 6 and 7e).

3. Syndepositional kink folds with 030° axes occur in zones $\leq$20 m wide.

4. Numerous outcrop-scale normal-sinistral and normal-dextral faults show clear upward termination indicating activity during deposition of Unit 2, yet some faults locally cut the younger upper Pliocene Poros Formation.

[19] The above observations indicate that 020°–040° D2 faulting started between deposition of Units 1 and 2 as mid-Pliocene fault activity that shifted the Apolakkia basin to a more northeast-southwest trend (Figure 3). Magnetostratigraphy of a faulted section including the oldest exposed Unit 2 strata ("AP" in Figure 5) revealed a long reversed-polarity interval assigned to the Gilbert Chron [*van Vugt*, 2000]. On the basis of this correlation and the observation that 030° faults also cut the Poros unit, faulting occurred between ~5 Ma and the latest Pliocene (1.8 Ma), although yet younger activity cannot be excluded (Figure 3).

[20] The consistent proximity between inclined 030° basin margin normal faults and observed folds suggests a genetic relationship and that both are the product of extension rather than a regional shortening event. If the folding were the product of oblique- or strike-slip faulting, the fold axes would likely strike obliquely to the basin margin faults [e.g., *Christie-Blick and Biddle*, 1985; *Schlische*, 1995].

3.4. 050°–070° Basin-Scale Oblique-Slip Faults

[21] The 050°–070° structures are regionally significant major structures that bound both the modern basin margins

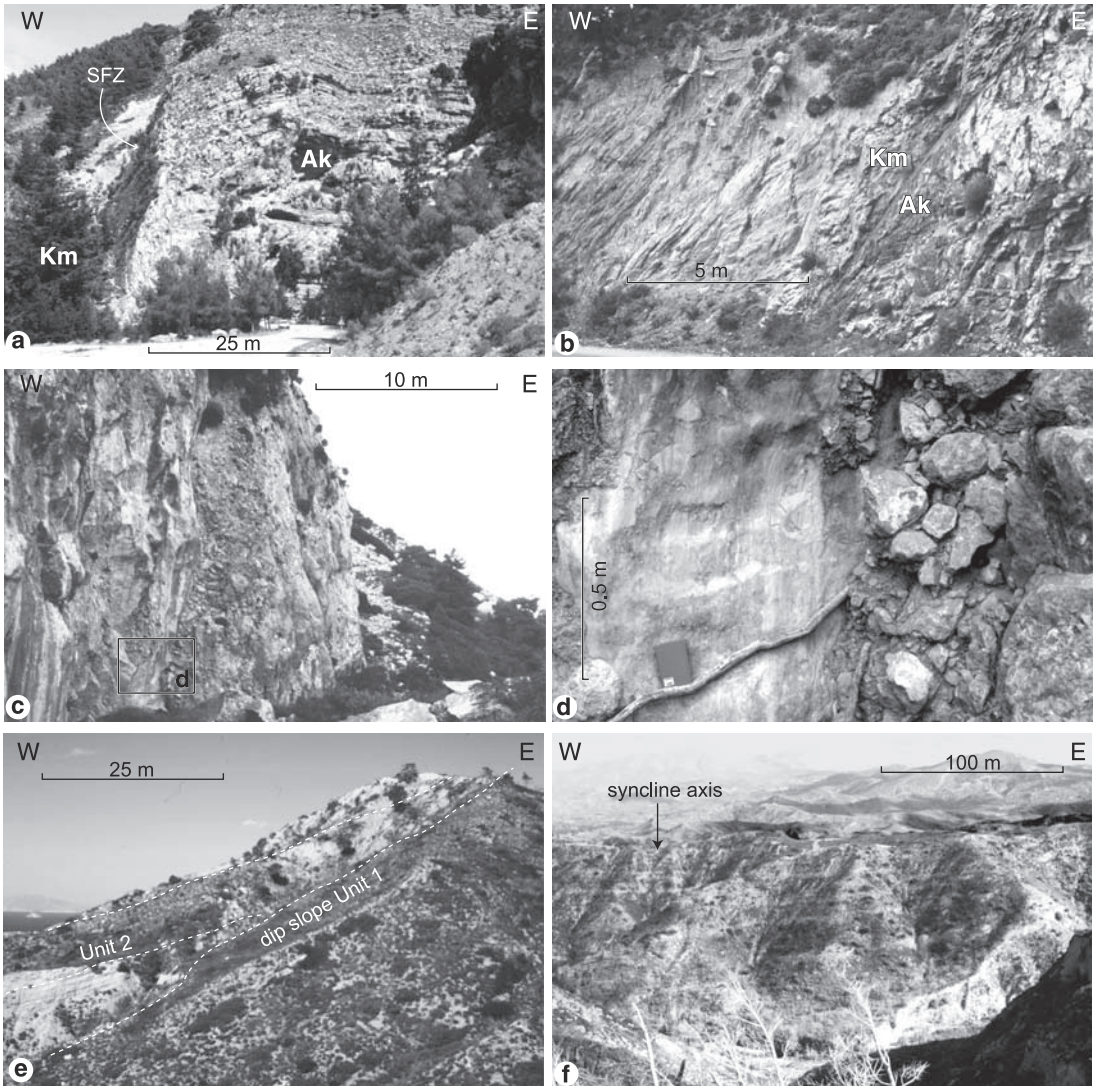

Figure 7. Deformation associated with basin-scale 020°–040° faults. For locations see Figure 5. (a) Easternmost fault of the Siana fault zone (SFZ) juxtaposing Kakoskala (Km) and Akramitis limestones (Ak) at the western limit of Mt. Ataviros. A 30-m-wide anticlinal drag fold developed in well-stratified Ak in the footwall. (b) Approximately 1 km south of Figure 7a, highly deformed, relatively soft Km deposits in the hanging wall display sigmoidal deformation indicative of nearly pure dip slip. (c) Subvertical fault plane at westernmost fault of the SFZ. Inset shows area of detail shown in Figure 7d. (d) Subvertical groove marks and fault breccias adhere to the SFZ fault. (e) Angular unconformity of ~20° between clastic deposits of Unit 1 and Unit 2 near Moni Skiathi. (f) West dipping, eastern limb of the syncline near Arnitha shows fanning dips with progressive decrease in dip upward, indicative of syndepositional deformation.

and are expressed throughout the basin and surrounding basement (Figure 5). The 050°–070° lineaments displaced 030° lineaments in the satellite images (Figure 4), suggesting that although both fault populations are components of D2, the 050°–070° faults were initiated after the 020°–040° faults (Figure 3).

[22] Observations along the northern basin margin indicate that slip varied between dominantly dip slip (Figure 8c) to sinistral-oblique slip on different fault segments (Table 1). For example, the basin's northern boundary is a subvertical 070°-trending fault zone, the Monolithos–Aghios Isidoris fault zone (MAIFZ; Figures 5 and 8a–8c), along which the basement also displays 070° lineaments (Figure 4). The MAIFZ is locally demarcated by pronounced ridges of vertically dipping fault breccias and cataclastic basement limestones (Figures 8d–8f). In the northwestern basin (Figure 5), syncline axes lie along strike with the exposed MAIFZ, suggesting that the folds are not contractional but are fault-parallel drag folds generated by dip slip along locally blind 070° faults (usage of *Suppe and Medwedeff* [1990]).

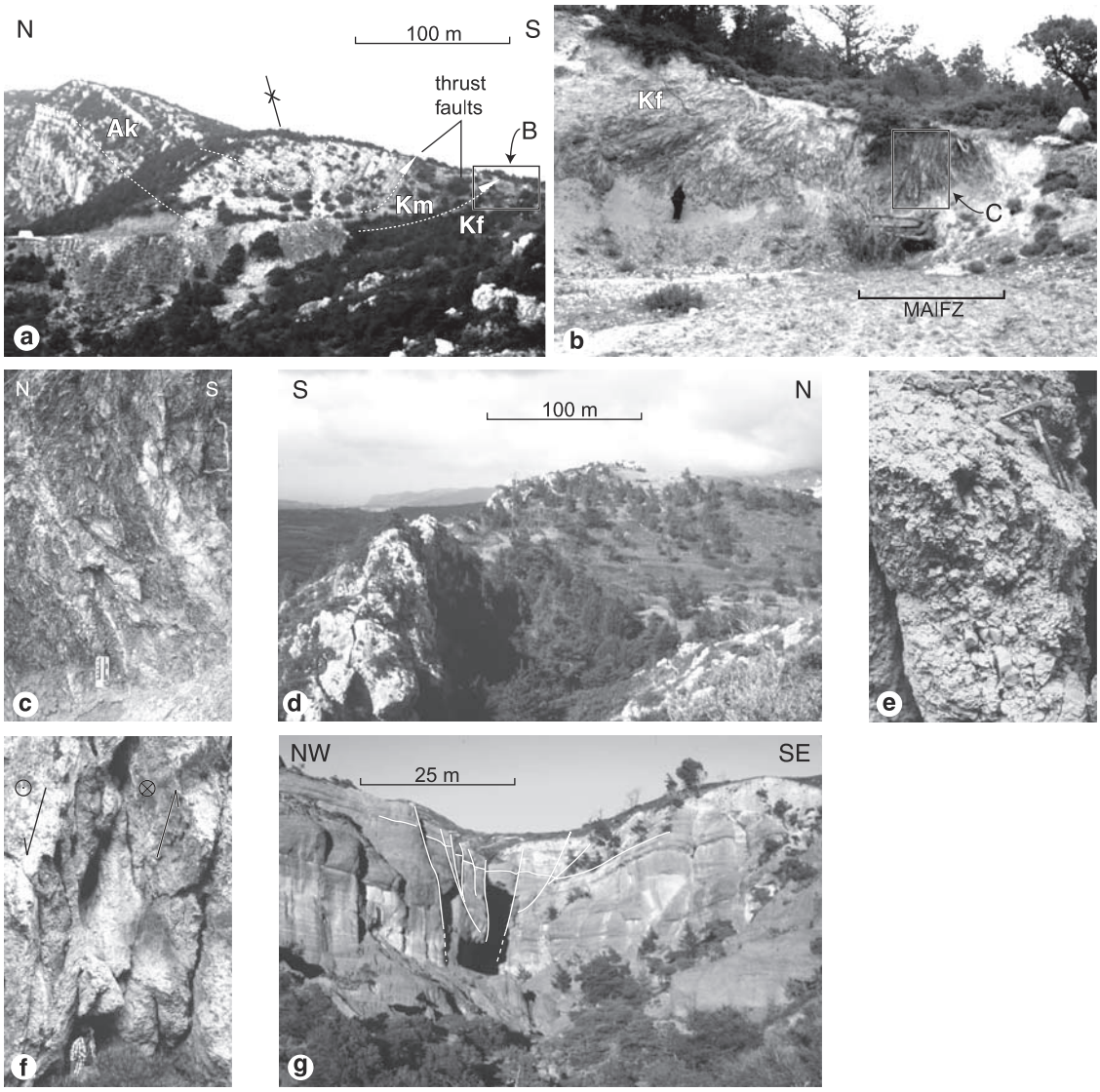

Figure 8. Deformation associated with basin-scale faults of the 050°–070° population. For localities see Figure 5. (a) West of Monolithos, the MAIFZ displaced a sequence of older north dipping, south vergent basement thrusts separating the Akramitis limestone (Ak), Kakoskala limestone (Km), and Katavia flysch (Kf). (b) Detail of Figure 8a showing the subvertical MAIFZ cutting the chaotically deformed Katavia flysch. Note person for scale. (c) Detail of Figure 8b showing steeply south dipping shear fabric along decimeter-scale sigmoids of white marl. Left-hand scale is in centimeters. (d) Prominent narrow, steep ridges with vertically dipping fault breccias and cataclastic basement limestones that demarcate subvertical 070° shear zones within the MAIFZ, east of Siana. (e) Detail of vertically dipping fault breccias within limestone ridge of Figure 8d. (f) Large subvertical sigmoids within the MAIFZ shear zone at Figure 8d indicative of sinistral-oblique displacement; person for scale at bottom. (g) Proposed 060°-trending negative flower structure southwest of Arnitha (white lines) delineated by a few meters of vertical offset of Vati conglomerates.

The westward plunge of the syncline at Cape Fourni (Figure 5) may reflect subordinate wrenching on the subsurface MAIFZ. Such synclines above shear zones are the surface expression of negative flower structures observed in seismic profiles (Figure 8g) [e.g., *Harding et al.*, 1985; *Lowell*, 1985]. No indications for 050°–070° faulting during Unit 1 deposition were observed, but the onset of 050°–070° faulting occurred after the onset of Unit 2 deposition (Figure 3). Along the southernmost basin boundary, paleosols of Unit 2 onlapped the basement flysch only to be faulted later (Aspropetres fault zone (AFZ); Figure 5). In the northwestern basin, steep sinistral-normal faults related to the MAIFZ are expressed in lower Unit 2 as faulted conglomerate clasts, but dragged the overlying travertine subunit of Unit 2 vertically.

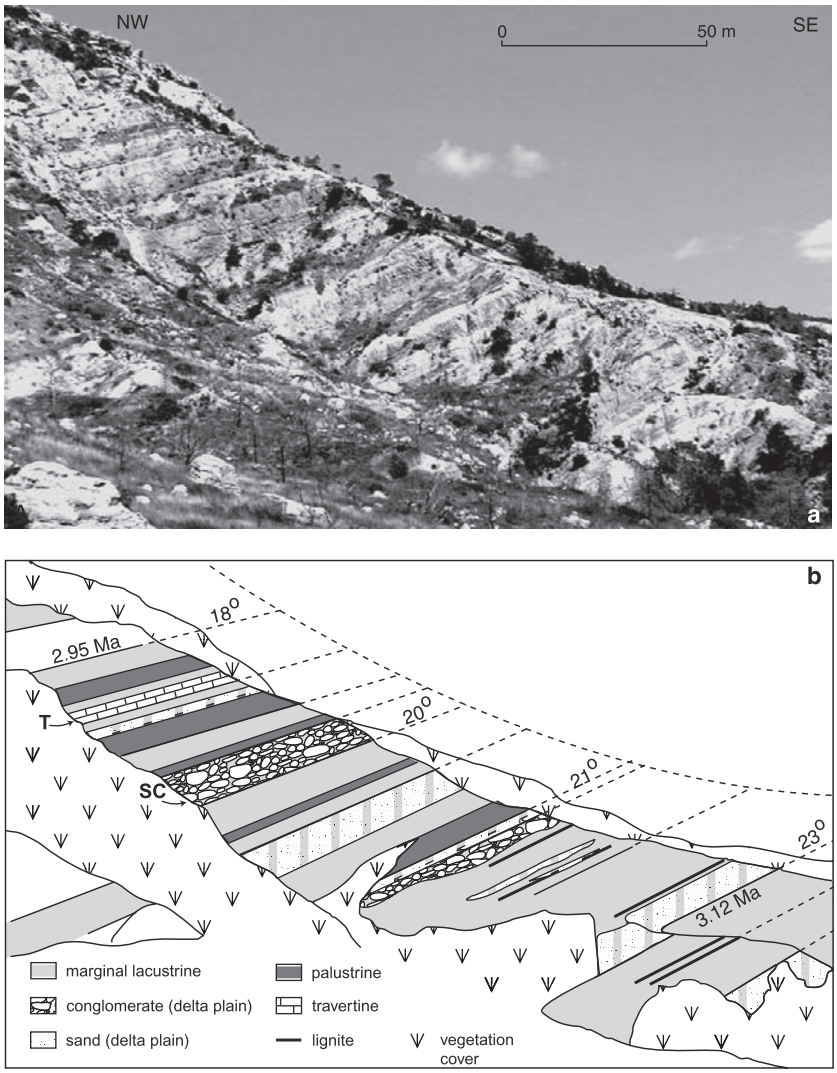

Figure 9. (a) Photo illustrating fanning dips generated by syndepositional folding in the southern limb of the Monolithos syncline, near Cape Fourni ("M" in Figure 5). (b) Interpretation of Figure 9a showing decreasing dip magnitudes stratigraphically upward. Abbreviations are as follows: SC, sandy conglomerate bed; T, lowermost travertine bed.

Fault displacement decreases upward, and the uppermost travertine strata cover these faults (cross section CC′; Figure 6). Unit 2 gravels were likely confined to the basin margin by fault-generated subsidence, and their ~40° dips likely reflect both initial depositional slopes of 12°–20° in the apical regions of alluvial fans [*Blair and McPherson*, 1994] plus tectonic tilting. Stratigraphically higher strata, whose age is 3.15–2.9 Ma ("M" on Figure 5) [*van Vugt*, 2000], display fanning dips due to syndepositional activity on the MAIFZ (Figure 9). Farther south in the same fold limb ("AG" on Figure 5), the maximum age of syndepositional deformation is ~3.5 Ma recorded by the Gilbert-Gauss transition [*van Vugt*, 2000]. Fanning dips related to 050°–070° faults are absent in the oldest Unit 2 strata.

[23] Using the magnetostratigraphically derived ages of ~3.5–2.95 Ma for folded Unit 2 sedimentary cycles [*van Vugt*, 2000], a calculated tilting rate of ~0.03°/kyr corresponds to a vertical-slip rate of ~87 cm/kyr on the MAIFZ to accommodate the 550 m of Unit 2 deposited in that time interval. That undated travertine deposits stratigraphically above profile "M" are also folded demonstrates that syndepositional folding and shear on the MAIFZ continued after 2.95 Ma. Pleistocene or younger activity led to an additional 10–20 m vertical offset of the upper Pliocene Poros across the MAIFZ. Continued Holocene activity is likely given the orientations of modern river valleys and mountain ridges.

3.5. 160°–180° Outcrop-Scale Oblique Faults

[24] Faults with normal-dextral or dextral-oblique displacement dominate over faults with a sinistral sense in the 160°–180° fault population, although all faults have a principal dip-slip component (Table 1). For example, 170° faults displaced cobble segments in Unit 2 conglomerates and ductilely deformed marl intraclasts ("SC" in Figure 9b),

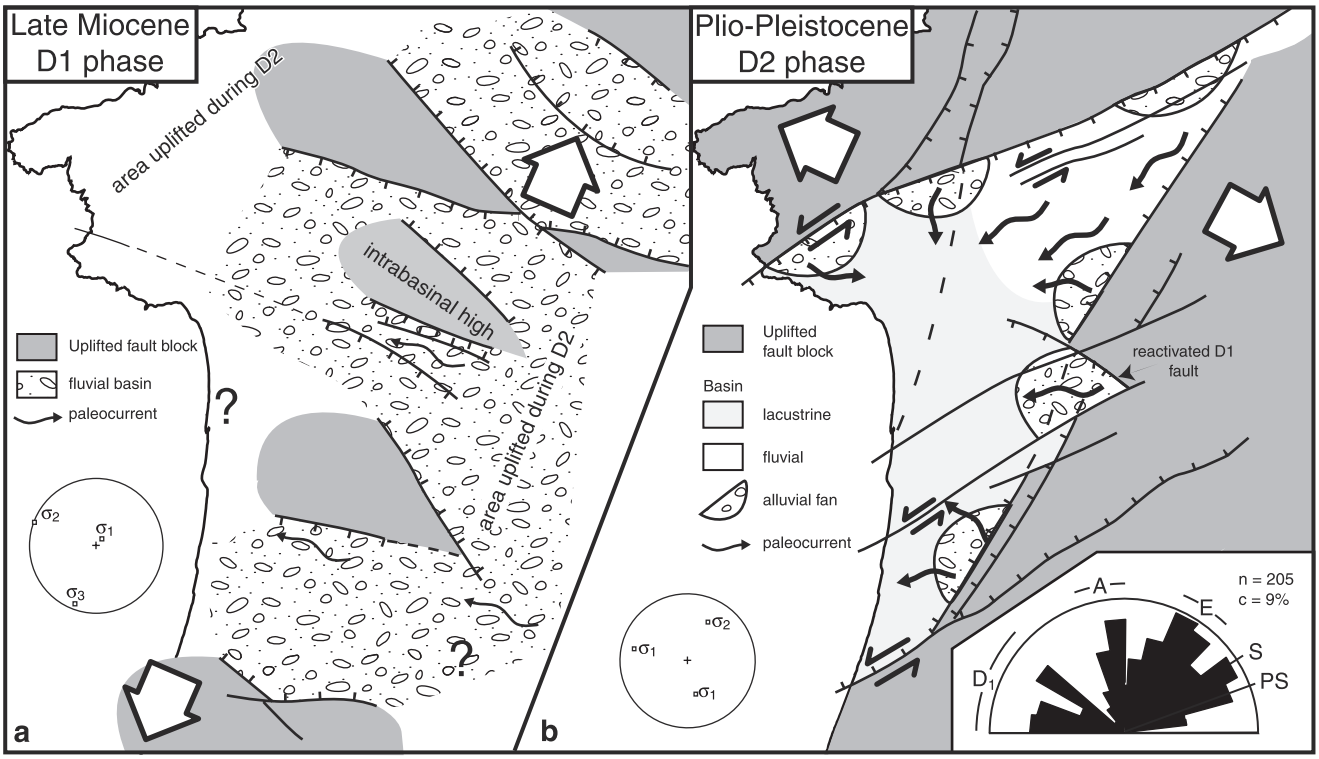

Figure 10. Paleogeographic reconstruction of the Apolakkia basin during (a) late Miocene D1 deformation phase and (b) Plio-Pleistocene D2 deformation phase. The outcrop scale of 160°–180° faults precludes their being shown. White arrows indicate maximum extension direction based on stress inversion of mesoscale fault data ("σ_3" in Figures 13e and 13f). Inset shows interpretation of 205 mesoscale faults. Inset abbreviations are as follows: PS, primary synthetic fault; S, synthetic faults; E, extensional (normal) faults; A, antithetic faults (usage of *Smith and Durney* [1992]); D_1, all faults that developed during D1 deformation.

indicating that faulting occurred when the channel deposits were unconsolidated. The lowermost travertine bed locally appears unaffected by these 170° faults ("T" in Figure 9b), suggesting that faulting ceased prior to ~2.95 Ma [*van Vugt*, 2000]. However, other 160°–180° faults cut the Poros, indicating that although fault activity started in late Pliocene time, it continued elsewhere beyond the Pliocene-Quaternary boundary (Figure 3). Outcrop-scale 020°–040° and 160°–180° faults often display a conjugate relationship, suggesting that although the 020°–040° population became active earlier, it remained active simultaneously with the 160°–180° population until after latest Pliocene time.

[25] The D2 deformation phase thus consisted of three fault populations active simultaneously in Plio-Pleistocene time. The normal-dextral or dextral-oblique displacement that dominated the 160°–180° population complemented the 020°–040° normal faults and 050°–070° sinistral-oblique system in response to apparent northwest-southeast extension (Figure 10b). Thus subsidence and filling of the Apolakkia basin during both phases D1 and D2 occurred under local fault control, but the D2 phase resulted in reorientation of the basin axis to its present northeast-southwest trend, reflecting a significant kinematic change from late Miocene northeast-southwest extension (Figures 3 and 10a).

[26] Facies architecture and paleocurrents of Unit 2 suggest that the modern southeastern basin margin closely corresponds to the Pliocene margin controlled by syndepositional 020°–040° normal faults. Clast imbrication data indicate that Unit 2 gravels along the southeastern margin of the basin were derived from the east. However, the maturity of these deposits and an absence of indicators of steep fans suggest that the basin margin had gentle relief even though it was a sediment source. The absence of vertical facies trends or trends reflecting an apparent rise in the water table during deposition of fluvial Unit 2 implies that sedimentation rates were balanced with subsidence rates [*Duranti*, 1997; *Kovacs and Spjeldnaes*, 1999].

[27] Along the basin's northern margin, the oldest Unit 2 gravels locally onlapped the basement flysch prior to 050°–070° faulting with clast imbrication data indicating a north-northwestern provenance [*Duranti*, 1997]. Thus opposing paleocurrents along the southeastern and northern basin margins plus our fault observations lead us to infer a half graben basin geometry [cf. *Leeder and Gawthorpe*, 1987] during D2 faulting with both footwall and hanging wall alluvial-fan and fluvio-deltaic systems feeding the basin (Figure 10). Maximum subsidence occurred along the

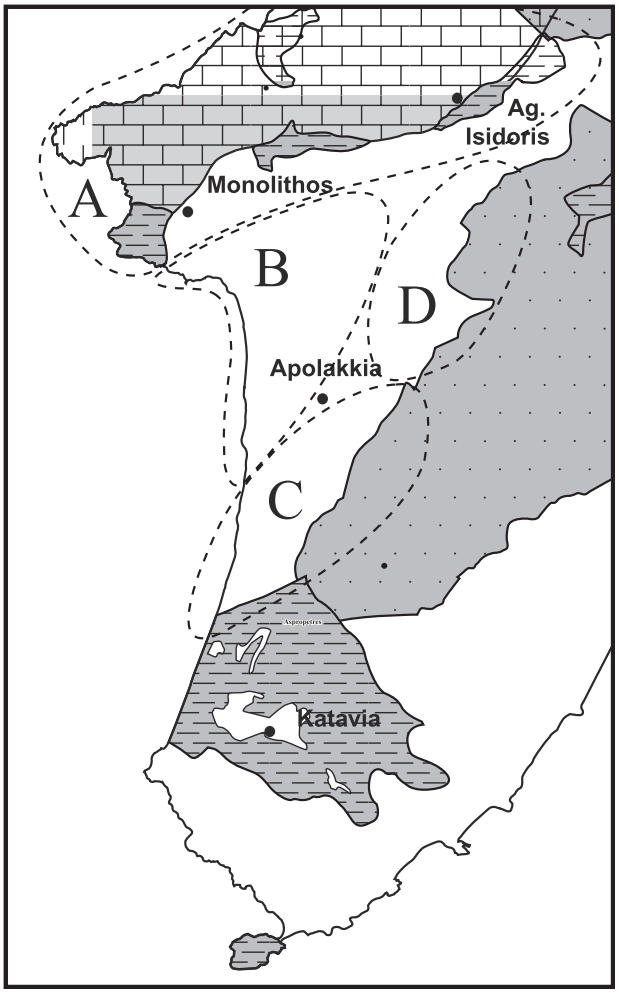

Figure 11. Locality map of the structural domains defined within the Apolakkia basin for mesoscale fault analysis.

northern margin, and we speculate that the subvertical MAIFZ may mark a listric master detachment at depth.

4. Analysis of Mesoscale Fault Slip Data

4.1. Methods for Analyzing Fault Slip Data

[28] Slip data from mesoscale faults are also analyzed in comparison to the basin-scale faults discussed in section 3 to test the reproducibility of the kinematic interpretations and to better test for any component of transtension recorded by the D1 and D2 structures. Mesoscale faults that either border or intersect the Apolakkia basin yielded 205 fault slip data. Slickensides, groove marks, and mineral fiber growth directions were measured as field kinematic indicators. The principal stresses responsible for the generation and subsequent deformation of the basin were interpreted using stress inversion procedures as initially described by *Angelier and Mechler* [1977]. Calculations were done with the program TectonicVB 1.3 (a program for analysis of orientation data) of H. Ortner (1991), whereas graphical presentations of the fault slip data were generated using the program Faultkin 3.8a (a computer program for analysis of fault slip data), of R. A. Allmendinger et al. (1992).

[29] One of the main assumptions in stress inversion procedures is that the stress tensor acting on each fault was uniform and that slip was parallel to the resolved shear stress on each fault plane. However, in reality, measured fault populations are heterogeneous and result from the successive generation, reactivation, and rotation of faults throughout a deformation history [*Bruhn and Pavlis*, 1981; *Gapais et al.*, 2000]. Preexisting faults suffer the entire deformation history, whereas new faults may appear at any time during progressive deformation. Also, the spatial nonuniformity of a stress field (e.g., strike-slip-dominated deformation) may contribute to the heterogeneity of measured fault populations. Because magnitudes of slip are seldom quantifiable, faults are often given the same weight regardless of their magnitude of slip. However, as particular structural features are more pronounced at some scales than others, the simultaneous study of faults at more than one scale leads to a better understanding of the general deformation mechanism [*Tchalenko*, 1970].

[30] To counter the limitations described above, Apolakkia fault data were segregated into subsets, each tested independently. First, in order to address the spatial variation in fault data, the study area was divided geographically into four structural domains (labeled A–D; Figure 11). Domain A, in the northern part of the basin, is dominated by faults of the MAIFZ and the 030° normal faults separating basement massifs. The coastal badland area northwest of Apolakkia is domain B, a domain characterized by the predominance of 030° faults and extension-induced folds with few 070° faults transecting the domain. The southernmost part of the basin that was influenced by the activity of the 065°-trending AFZ and the 030° faults along the southeastern basin margin is assigned to domain C. Domain D is the area in the vicinity of Profilia and includes 100°–130°, 145–155°, 020°–040°, and 070° faults (Figure 5). The 160°–180° faults occur predominantly in the coastal areas of domains A and B.

[31] Second, to address the fault scale, the data were divided into a small suboutcrop scale, an intermediate outcrop scale, and large master faults. This subdivision also enables weighting of the faults according to their relative contribution to the deformation within the distinguished domains in the absence of estimates of slip magnitude. An arbitrary weighting ratio of 3:2:1 was applied to master faults, mesoscale faults, and small-scale faults, respectively. Weighting had minimal effect on the stress inversion results.

[32] The third subdivision based on age of faulting relied on crosscutting relations, syndepositional deformation, and/or the age of displaced rock units as summarized for the basin-scale faults in section 3 (Figure 3). Mesoscale faults whose trends were similar to a basin-scale fault population were assigned the age of that population. Sorting by age was done within the previously defined structural domains (A–D) to make it easier to determine the relative contribution of a certain phase to the overall deformation of the basin. This approach also enabled an assessment of the heterogeneity of stresses at the scale of the basin for the two recognized deformation phases.

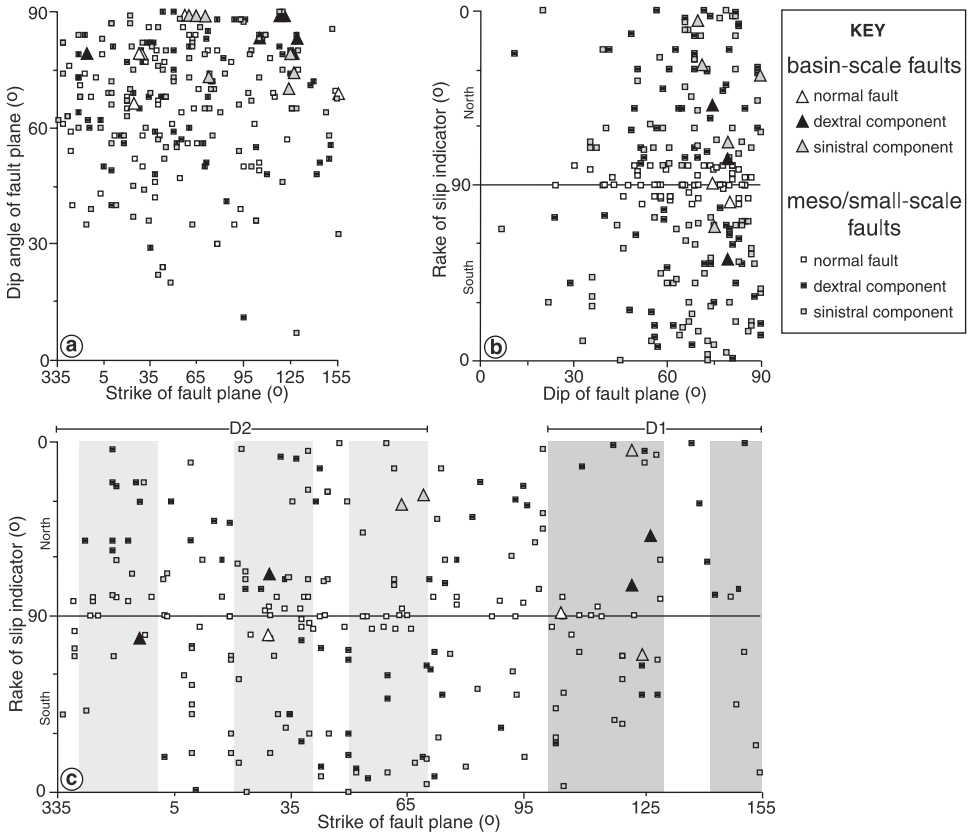

Figure 12. (a) Magnitudes of dip of 242 mesoscale and basin-scale fault planes are steep (70% $\geq 60°$) regardless of strike of the fault plane. (b) Rake of the slip indicator (plunging toward Northern or Southern Hemisphere) versus magnitude of fault plane dip showing that these 242 faults do not satisfy Coulomb theory. (c) Rake of the slip indicator (plunging toward Northern or Southern Hemisphere) versus strike of the fault plane with strikes of basin-scale fault populations shaded as D1 faults (dark shading) and D2 faults (light shading).

[33] In addition to stress inversion analyses, we applied a simple graphical method of *Célérier* [1995] and *Célérier and Séranne* [2001] to examine the strike-slip components of fault slip more closely. This method also relies on both the strike and dip of the fault plane and the slip orientation (usage of *Bott* [1959]) but allows an independent evaluation of any fault reactivation. A Breddin's graph is applied to the field data with rakes $\leq 80°$ as a series of curves for $\Phi \in [0,1]$ that represent the rakes as a function of fault plane strike for a fixed fault plane dip of 80°. This value represents the average dip of the master faults of the Apolakkia basin. By calculating a best fit curve for the field data [*Célérier and Séranne*, 2001], we derive both the orientation of the maximum principal horizontal stress and an estimate of the Φ value, indicating the tectonic regime where $\Phi = 1 - r_0$, $\Phi = \sigma_2 - \sigma_3 / \sigma_1 - \sigma_3$, and r_0 is the stress ratio parameter of *Célérier* [1995]. Although *Célérier*'s [1995] method was devised to predict rakes on preexisting fault planes, we use it to assess the complexity of our mesoscale fault data.

4.2. Summary and Interpretation of Results

[34] Regardless of their strike or timing of activity, the faults dip steeply including the dip-slip-dominated faults (Figure 12a). The basin-scale faults consistently dip >60° with an average dip of ~80°, whereas 70% of the mesoscale faults dip >60° with an average of ~65°. Also, the rakes are highly variable regardless of the dip of the fault plane (Figure 12b), implying that these faults do not satisfy Coulomb theory, which predicts an inverse relationship between the magnitudes of the rake and fault plane dip, but record three-dimensional strain (usage of *Reches and Dieterich* [1983]). Although the two deformation phases are clearly distinguishable based on map-scale structures, their distinction and that of discrete fault populations are less obvious in the mesoscale data because of a greater scatter in the strikes of fault planes (Figure 12c). However, stress analysis yields results that corroborate those of the basin-scale faults.

4.2.1. Phase D1

[35] Fault plane solutions, often used as a first approximation of the stresses [e.g., *Marrett and Allmendinger*, 1990], suggest that the stress regime responsible for D1 deformation was not homogeneous throughout the four domains but was characterized by north-northeast-south-southwest to north-east-southwest tension with T axes essentially subhorizontal and P axes subvertical (Figures 13a–13d). Closer examina-

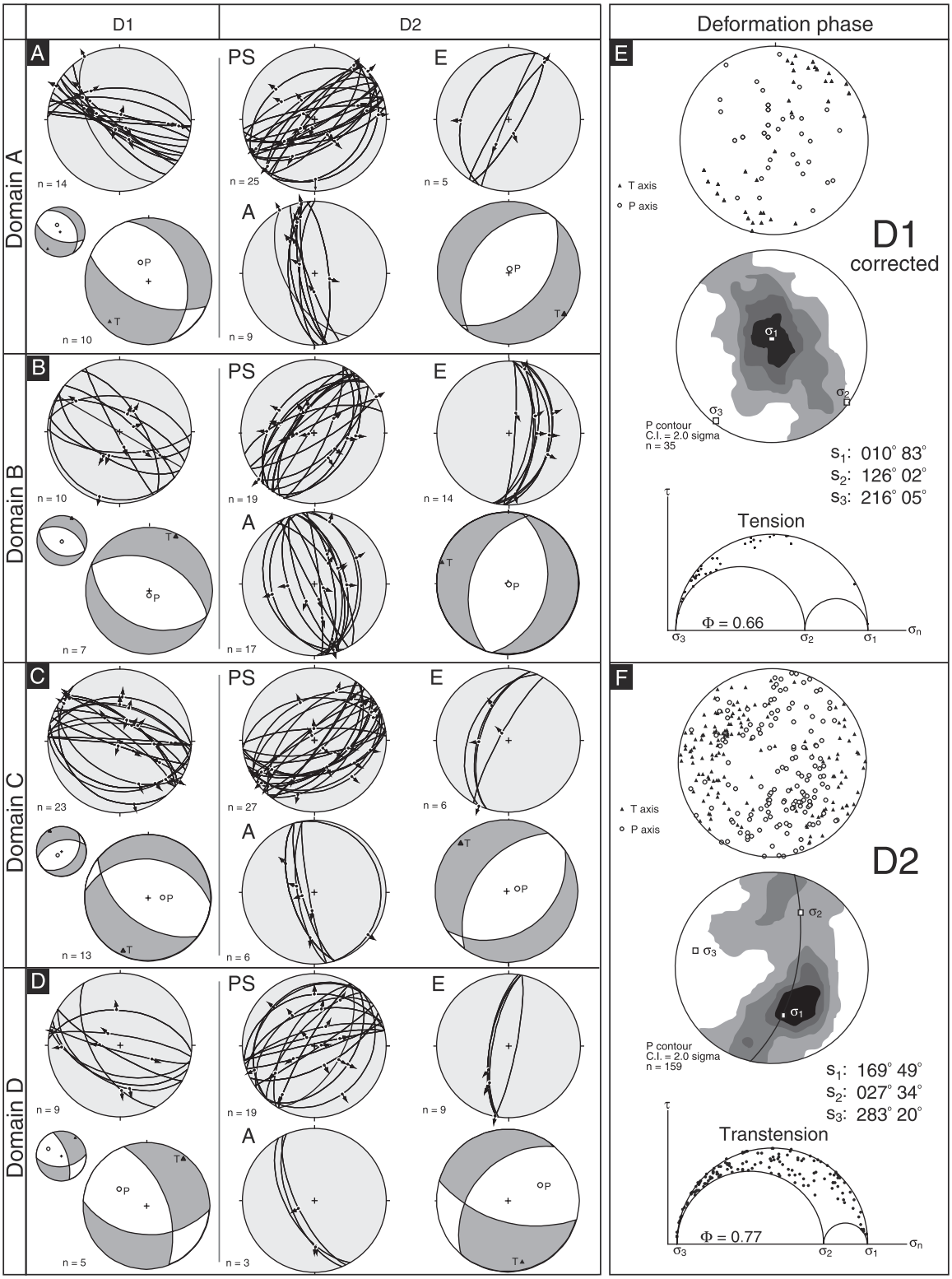
D1
D2
Deformation phase
Domain A
Domain B
Domain C
Domain D
A
B
C
D
E
F
PS
E
A
n = 14
n = 25
n = 5
n = 10
n = 9
n = 10
n = 19
n = 14
n = 7
n = 17
n = 23
n = 27
n = 6
n = 13
n = 6
n = 9
n = 19
n = 9
n = 5
n = 3
T axis
P axis
D1
corrected
P contour
C.I. = 2.0 sigma
n = 35
s1: 010° 83°
s2: 126° 02°
s3: 216° 05°
Tension
Φ = 0.66
D2
P contour
C.I. = 2.0 sigma
n = 159
s1: 169° 49°
s2: 027° 34°
s3: 283° 20°
Transtension
Φ = 0.77

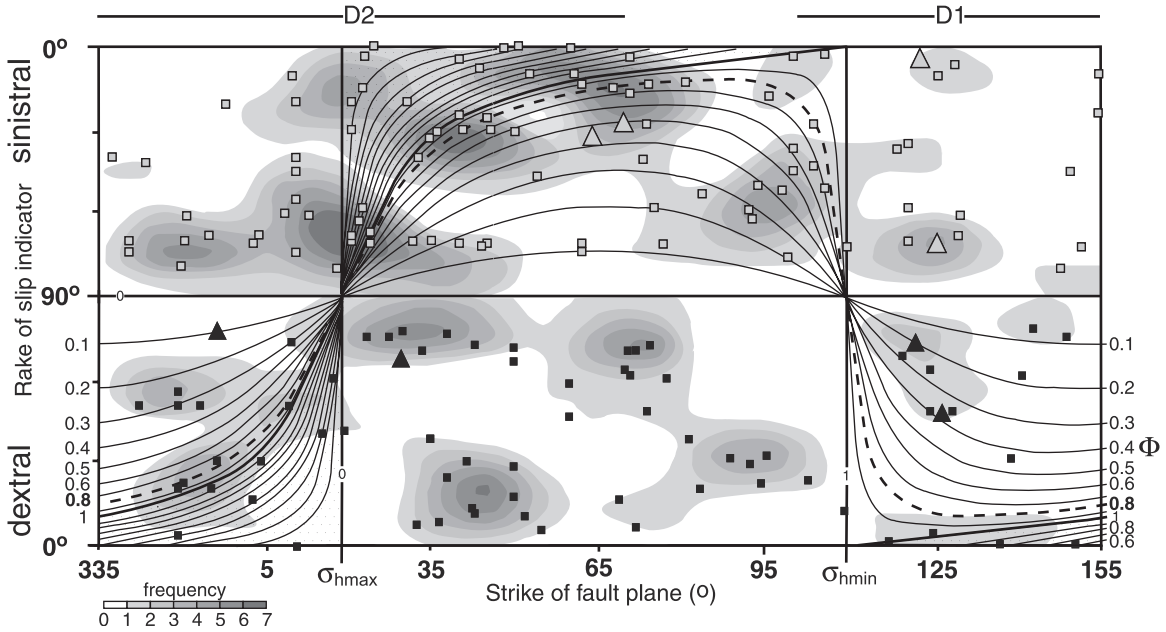

Figure 14. Strike of the Apolakkia basin fault planes versus rake of the slip indicator for rakes <80° (symbols as in Figure 12). Data points are contoured with a nearest-neighbor interpolation using a 10° grid spacing for both axes (fault strike and rake). Superimposed on the data is a Breddin's graph for fixed fault planes dipping ≥80°, showing a relationship between rake and fault strike as calculated by *Célérier* [1995]. The solid curves represent values of Φ from 0 to 1 in increments of 0.1. Bold solid line denotes Φ = 1 (pure wrench), and bold dashed line represents Φ = 0.8 (transtension), the best fit for Apolakkia fault data. Lightly stippled zones correspond to wrench faulting; extensional regime is not stippled. D1 and D2 indicate the orientations of the corresponding basin-scale fault populations.

tion reveals that strike-slip faults represent ~35% of the D1 structural assemblage but give a stress inversion that agrees better with that of the D2 structural assemblage, i.e., with northwest-southeast tension, making it likely that these D1 faults were reactivated during the younger D2 phase. Such an interpretation is supported further as these dextral strike-slip faults satisfy the best fit D2 curve of the Breddin's graph (Figure 14). Mesoscale D1 faults along the D2-controlled southeastern basin margin (domain C) were most sensitive to reactivation during phase D2, and they may have originated as D1 dip-slip faults more akin to the basin-scale fault wedge array (Table 1 and Figure 10).

[36] After subtraction of the faults that are kinematically compatible with phase D2, fault plane solutions indicate more homogeneous D1 stresses over the entire basin, characterized by northeast-southwest tension with T subhorizontal and P subvertical (Figures 13a–13d). Using the corrected D1 data from all domains (Figures 13a–13d), a best fit stress inversion yields a σ_3 that plunges gently toward 216° and a maximum compression σ_1 plunging subvertically toward 010° (Figure 13e), results that are consistent with the basin-scale faults (Figure 10). The stress-ellipsoid shape parameter $\Phi = 0.66$, in conjunction with the stress axes, indicates plane stress under northeast-southwest D1 extension (Figure 13e).

4.2.2. Phase D2

[37] D2 faults are dominated by a sinuous trend of rakes from dextral strike-slip faults at 355° to sinistral strike-slip faults striking 070° (Figure 14). Thus the strike-slip com-

Figure 13. (opposite) (a–d) Lower hemisphere equal-area stereo projections for mesoscale fault data in the structural domains A–D of Figure 11. Senses of slip on the fault planes are represented by arrows. Fault plane solutions were calculated for the D1 and D2 structural assemblages in all four domains, with shading representing tension and white representing compression. For D1 faults, small fault plane solutions represent all measured faults within a domain, whereas large plots show subsets corrected for faults kinematically compatible with D2 stresses, i.e., reactivated faults. Abbreviations are as in Figure 10 inset. (e and f) P (open circles) and T (solid triangles) scatterplots for both deformation phases, together with plots in which P axes are contoured to represent the orientations of the principal stress axes. Mohr circles delineate the best fit models for the D1 and D2 tectonic regimes with $\Phi = 1 - r_0$ [*Célérier*, 1995]. Stress inversion analyses employed TectonicVB 1.3 (a program for analysis of orientation data, of H. Ortner, 1991), and graphical presentations of the fault slip data were generated using Faultkin 3.8a (a computer program for analysis of fault slip data, of R. A. Allmendinger et al., 1992).

ponent decreases clockwise from the 355° orientation with pure normal faulting approached at ~020°. At azimuths 020°–105°, the strike-slip component again increases in the contoured data with sinistral-oblique faults in the 020°–050° range and sinistral faults in the 050°–070° range. At strikes >070°, faults record a stronger dip-slip component. This sinuous trend in the contoured data best fits rakes predicted for $\Phi = 0.8$ with the maximum principal horizontal stress (σ_{hmax}) trending 020° and the minimum principal horizontal stress (σ_{hmin}) trending 105° (Figure 14). Rakes on the dextral strike-slip faults of the D1 assemblage are also consistent with the $\Phi = 0.8$ curve, strongly suggesting their reactivation. D1 faults dominated by dip slip do not fit the same curve further suggesting a lack of synchronicity. Following *Célérier* [1995], the best fit $\Phi = 0.8$ curve is consistent with a sinistral transtensional D2 tectonic regime.

[38] Not all D2 field data satisfy the best fit $\Phi = 0.8$ curve as illustrated by dextral and sinistral slip having occurred simultaneously on faults with approximately similar strikes (Figure 14). Such behavior typified the mesoscale and small-scale structures, suggesting that smaller anastomosing faults may reflect relative rates of motion of individual fault slivers, either synthetic or antithetic, within larger basin-scale shear zones. Within both the sinistral and dextral fields (Figure 14), gaps between loci of faults with the same strikes suggest that oblique stresses were partitioned between wrench-dominated faults versus dip-slip-dominated faults.

[39] Cumulative fault plane solutions for the Plio-Pleistocene D2 phase are characterized by west-northwest-south-southeast tension with a subhorizontal T axis and a moderately dipping P axis (Figure 13f). The similarity among fault plane solutions for all four domains also indicates homogenous D2 strain throughout the entire basin (Figures 13a–13d). The best fit stress inversion yields a σ_3 axis that plunges slightly toward 283° and a σ_1 axis plunging moderately toward 169° with $\Phi = 0.77$ (Figure 13f). This best fit Φ value mimics the $\Phi = 0.8$ predicted from the Breddin's graph (Figure 14), which together with the stress axes reinforces the view that the D2 phase was transtensional. The orientations of σ_2 and σ_3 (Figure 13f) correspond closely to those of σ_{hmax} and σ_{hmin}, respectively (Figure 14), leading us to examine the significance of these orientations more closely.

5. Basin-Scale Faults and Models for Transtension

[40] Given that the mesoscale-fault data suggest D2 sinistral transtension, the basin-scale results also should be tested for a record of transtension. Field evidence for the highest strain along the MAIFZ (Figure 5) and throughout the basin on 050°–070° faults suggests that this population constitutes the primary synthetic D2 faults (PS) of the Apolakkia basin (Figures 13a–13d). Experimental studies of oblique divergence by *Smith and Durney* [1992] show that the angle (2Θ) between the strikes of synthetic faults (PS) and the strikes of the antithetic faults (A) decreases as the displacement angle varies from $\alpha = 0°$ (pure wrench) to $\alpha = 90°$ (pure divergence). Of the D2 faults, the 020°–040° normal faults correspond best to the predicted orientations of normal faults (E) for $\alpha = 30°$, and the 160°–180° dextral-normal faults correspond to the predicted orientations of antithetic faults (A) for $\alpha = 20°$ (Figures 10b (inset) and 13a–13d). The Apolakkia basin also exemplifies fault trends that agree with the sinistral transtension experiments of *Withjack and Jamison* [1986] and *Clifton et al.* [2000], showing that if $\alpha = 30°$, dextral strike-slip and normal faults develop at angles of ~60° and ~30° to the PS trend, respectively (Figure 10b inset). *Withjack and Jamison* [1986] also found that for $\alpha = 30°$, synthetic faults experience combined normal and sinistral strike slip, whereas pure strike slip dominates if $\alpha = 15°$. Because the Apolakkia 050°–070° faults record strong dip-slip components, we can place a lower limit on the divergence angle and infer that $\alpha = \sim 15° - 30°$ in D2 time.

[41] *Fossen and Tikoff* [1998] showed that the transition between pure-shear-dominated and wrench-dominated transpression (as the inverse of transtension) occurs at $\alpha = 20°$, implying that pure strike-slip faulting is restricted to $\alpha < 20°$ unless preexisting structures exist. This threshold of α falls within the Apolakkia range of $\alpha = 15° - 30°$. We use the Fossen and Tikoff criteria and the observations that the PS faults record significant dip-slip components (Figure 12c) to further delimit the D2 displacement angle to $\alpha = 20° - 30°$ and conclude that the basin-scale faults also indicate that Apolakkia basin responded to D2 transtension.

[42] The predicted angle between the PS and synthetic faults (S) when $\alpha = 20° - 30°$ ranges between 9°–12° [cf. *Smith and Durney*, 1992], predicting that Apolakkia basin S faults would have strikes of 058°–061°. These azimuths fall within the observed range of 050°–070° faults (Figures 10b (inset) and 13a–13d), suggesting that such subsidiary synthetic (S) faults are likely incorporated within this fault population. In the satellite imagery, 070° lineaments appear to bound zones of 050° lineaments (Figure 4, inset "b"), suggesting that the 050° structures are S faults formed as secondary structures synthetic to the PS faults.

[43] The established age of faulting shows that the 020°–040° normal faults (E) developed first and were followed by the synthetic 050°–070° PS faults and S faults, only to be followed last by the 160°–180° antithetic (A) faults (Figures 3 and 10b inset). A similar sequence of faulting emerged in various transtension experiments [e.g., *Tron and Brun*, 1991; *Smith and Durney*, 1992], indicating that not only are the trends of the Apolakkia basin-scale faults consistent with transtension but the sequence of their development also mimics that predicted by transtension experiments.

6. Relationship Between Offshore and Onshore Forearc Kinematics

[44] Data from the offshore Hellenic forearc are key to assess the broader significance of the structural relations observed onshore in the Apolakkia basin (Figure 15). Seismic reflection data and bathymetric trends on the continental slopes around Rhodes [*Mascle et al.*, 1986] and in the deep-marine Rhodes basin [*Woodside et al.*, 2000] reveal a predominance of major 070°-trending structures and scarps both onshore and offshore (Figure 15), suggesting they are regional inner-forearc shear zones over which sinistral trans-

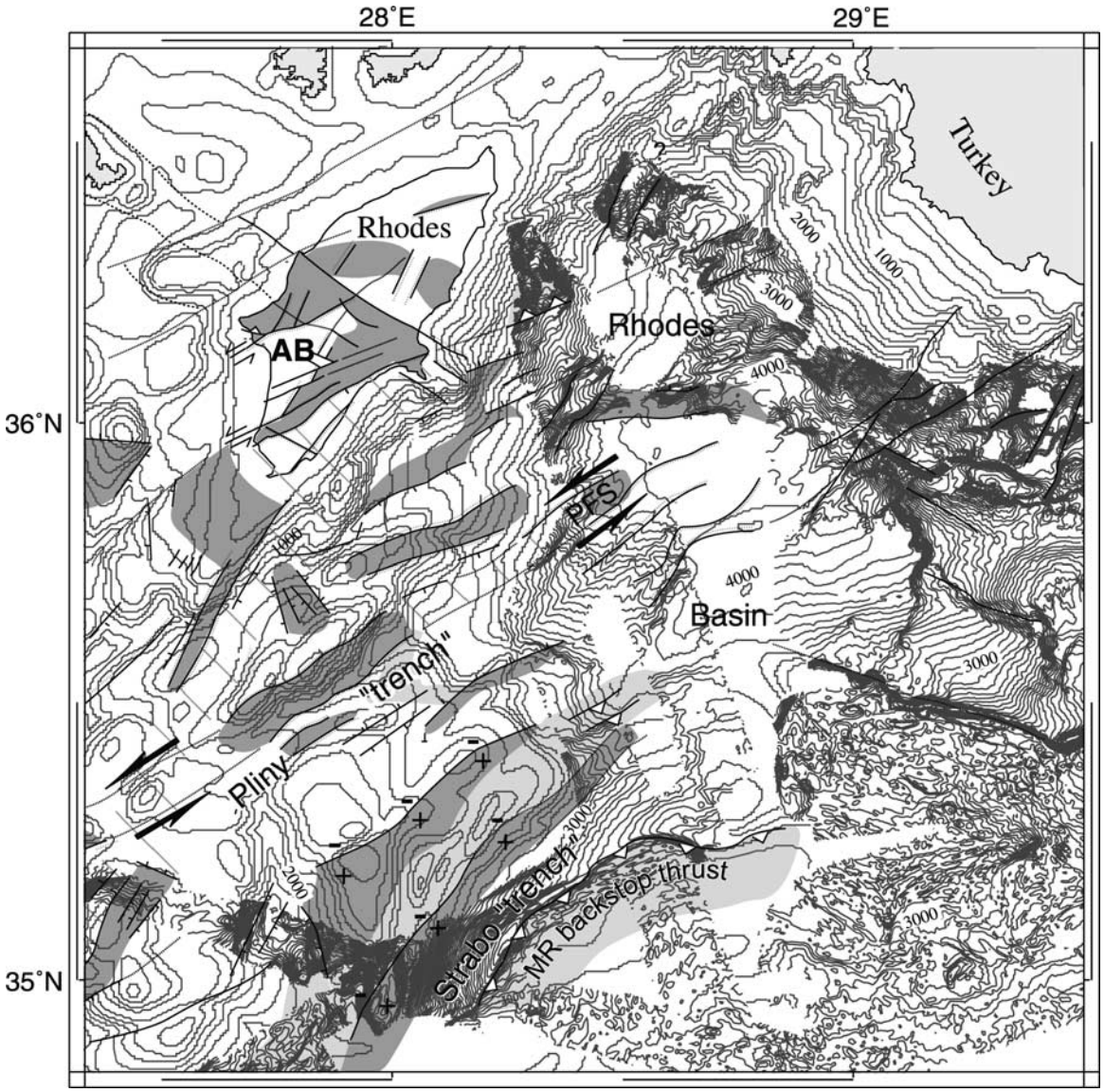

Figure 15. Tectonic elements of the studied Apolakkia basin (AB) compared to other areas onshore on Rhodes [*Mutti et al.*, 1970; D. Sakellariou, personal communication, 2000] and offshore in the adjacent Hellenic forearc [*Mascle et al.*, 1986; *Woodside et al.*, 2000]. Dark shading represents (sub)outcropping basement; light shaded areas are thrust nappes in upper Miocene-Quaternary strata; white areas represent Pliocene-Quaternary basins in the studied region. Thin lines represent structures consistent with D1 deformation; thick lines represent structures associated with D2 deformation. Plus and minus symbols are bathymetric highs and lows, respectively, with teeth on the overthrust block. ''PFS'' indicates positive flower structure in the northern margin of the Pliny ''trench'' [*Woodside et al.*, 2000]. MR is the active accretionary wedge of the Mediterranean Ridge. Bathymetry of the Rhodes basin at 50-m contour intervals is reproduced with permission from *Woodside et al.* [2000] and superimposed on 200 m contours [*IOC-UNESCO*, 1981].

tension has been resolved (Figure 13). The offshore 070° structures also appear to cut across structures with other trends, suggesting a regionally consistent sequence of faulting with young 070° structures as in the Apolakkia basin. In the central part of the Rhodes basin a positive flower structure marks the northern margin of the Pliny trench (PFS on Figure 15) [*Woodside et al.*, 2000], which together with its 070° linear morphology and en echelon subbasins suggest a post-Miocene sinistral-slip history for the aseismic Pliny trench [*Huchon et al.*, 1982; *Le Pichon et al.*, 1995].

[45] Other fault trends similar to those onshore on Rhodes occur throughout the inner forearc but are sparser. On the basis of bathymetric scarps and/or seismic profiles, 100°–130° and 145°–155° faults of the D1 phase appear

limited to the continental slopes west of Rhodes and southeast of the Rhodes basin, where they may be continuations of the 120° fault zones demarcating the central basement massif on Rhodes (Figure 15). Faults of the 160°–180° group appear absent offshore (Figure 15) but occur onshore predominantly at outcrop scale, a scale below the resolution of marine geophysical methods. Numerous 030° bathymetric trends are evident in the continental slope south of Rhodes and between Rhodes and Turkey, whereas the Quaternary Rhodes basin lacks these trends. The Vati basement massif on Rhodes, delineated by 030° normal faults (Figures 2b, 5, and 15), also appears in seismic profiles south of Rhodes (Figure 15) [*Mascle et al.*, 1986]. This horst acted as an offshore sedimentary ''dam'' since presumed post-Miocene time [*Mascle et al.*, 1986], consistent with onshore observations that an emergent Vati massif separated the dispersal systems of the Pliocene Apolakkia and Lachania basins [*Duranti*, 1997]. Thus the offshore data reinforce the view that onshore 020°–040° normal faults are older than other D2 faults but mark the onset of D2 deformation during which the forearc underwent significant morphological and kinematic reorganization. Despite the lower resolution of the offshore methods, we conclude that Apolakkia basin shares strain patterns with the adjacent offshore Hellenic forearc, and we extend our kinematic discussion to the broader inner forearc.

7. Plio-Pleistocene Plate Kinematics of the Eastern Hellenic Forearc

[46] D1 southwest-northeast extension of Apolakkia basin was likely a response to late Miocene southward migration of the forearc and lengthening of the plate boundary as its curvature increased from a nearly east-west middle Miocene plate margin (Figures 1, 10a, and 15) [*Le Pichon and Angelier*, 1979; *Kissel and Laj*, 1988]. An important reconfiguration of the stress field occurred during the hiatus between the middle-upper Miocene Unit 1 and the Pliocene Unit 2, a hiatus of a maximum of 3 million years, such that by early Pliocene time (4–5 Ma) the Apolakkia basin was responding to the D2 deformation (Figure 3). By 3.5 Ma, transtension due to combined west-northwest-south-southeast extension and 070° sinistral shear fully controlled the basin's evolution (Figure 10b).

[47] This change coincided with the late Miocene collision of the Arabian promontory with Eurasia and subsequent counterclockwise rotation and westward extrusion of the Anatolian-Aegean block from the Arabian-Eurasian collision zone [*Le Pichon et al.*, 1995]. A corresponding outward ''jump'' of the Hellenic subduction zone and rapid increase in plate boundary curvature are recorded as outward migrating loci of arc magmatism, back arc extension, and a Pliocene-Holocene clockwise rotation of the western Hellenic forearc (Figure 1) [*Le Pichon*, 1982; *Fytikas et al.*, 1984; *Mercier et al.*, 1987; *Kissel and Laj*, 1988; *Walcott and White*, 1998]. This change produced simultaneous increasing curvature of the plate boundary, an adjustment of the plate convergence vectors, an outward shift in the absolute position of the plate boundary, and an arc-parallel lengthening of the forearc region, all of which are evaluated in light of results from the Apolakkia basin and offshore forearc.

[48] The convergence vector defining relative motion between the Hellenic forearc and the African plate (''HA'' on Figure 1) differs only slightly from that of the outward spread of the Hellenic forearc relative to Eurasia (''HE'' on Figure 1), suggesting that plate convergence obliquity and the slight northward African motion do not drive forearc kinematics. Oblique convergence (HA) would generate sinistral transpression in the forearc, a prediction supported by shortening throughout the accretionary wedge of the Mediterranean Ridge northwestward to the Pliny trench. However, farther inboard, the forearc, including onshore Rhodes, lacks a record of shortening (Figures 5 and 15). Correspondingly, the D2 extensional direction is inconsistent with that predicted by oblique convergence regardless of whether strain is partitioned or not partitioned (Figure 13; usage of *Teyssier et al.* [1995]). The observed transition in structural style occurs at the Pliny trench (Figure 15), suggesting this trough demarcated a boundary between a transtensional inner forearc sliver to the northwest and a transpressional outer forearc sliver to the southeast. Thus the forearc slivers appeared mechanically decoupled, and the studied inner forearc appears little affected by oblique convergence with Africa.

[49] Alternatively, D2 transtension is better attributed to deformation internal to the Hellenic forearc. As the Mio-Pliocene forearc expanded outward from Anatolia, increasing both its length and curvature (Figure 1), the forearc stretched both parallel to the plate boundary and relative to a point in the central Aegean realm. This combined stretching resolves into sinistral tangential shear and orthogonal tensional components across 070° structures in the eastern Hellenic forearc and yields a stretching direction consistent with the D2 kinematics of Apolakkia basin (283°; Figure 13f), as well as modern geodetic data [*McClusky et al.*, 2000]. Although the position and orientation of the eastern Hellenic plate boundary changed from ~070° at 5 Ma to ~055° by 1.8 Ma (Figure 1), the orientation of the main shear zones in the forearc remained at ~070° (Figures 5 and 15). This consistency indicates that the eastern Hellenic forearc did not undergo bulk tectonic rotation during Pliocene time, but internal counterclockwise rotations accommodated the sinistral component between 070° fault zones [*Duermeijer et al.*, 1998, 2000].

[50] The onset of the D2 kinematic phase at ~4–5 Ma suggests a threshold of obliquity was reached whereby the inner forearc experienced oblique divergence. Although the D2 Apolakkia data suggest a displacement angle (α) of 20°–30°, the data represent a cumulative record of α, not necessarily the obliquity at initial wrenching. We speculate that the threshold obliquity was likely a larger α more akin to the >45° threshold noted in experiments on oblique divergence [*Smith and Durney*, 1992].

[51] The Hellenic plate boundary displays geometric elements similar to other curved convergent plate boundaries, such as the Aleutian arc, the Sunda Arc, the Leeward Antilles arc, or Hikurangi subduction zone. However, its history of increasing arc curvature and expanding overriding plate make it distinct geodynamically, and the Hel-

lenic boundary offers additional insight into the spectrum of curved plate boundaries.

8. Conclusions

[52] The following points summarize our conclusions.

1. Five fault populations in the late Miocene-Pleistocene Apolakkia basin on Rhodes record two deformation phases, both of which are consistent with outward expansion of the Aegean-Anatolian block. The kinematic change at ~4–5 Ma is attributed to a threshold of obliquity whereby the inner forearc started to experience sinistral-oblique divergence as the leading edge of the expanding forearc became increasingly curved.

2. The Apolakkia basin originated as a late Miocene fault-wedge basin in response to syndepositional southwest-northeast D1 extension with similar strain patterns in the adjacent offshore Hellenic forearc.

3. The Plio-Pleistocene D2 phase reoriented the basin and marked a shift to transtension resulting in combined syndepositional west-northwest-east-southeast (283°) extension and 070° sinistral shear. The principal shear zones in the forearc occur at ~070°, both onshore and offshore, suggesting the eastern inner Hellenic forearc did not undergo bulk tectonic rotation, but blocks between the 070° shear zones experienced Pliocene counterclockwise rotations and dip-slip-dominated sinistral-oblique divergence as in the Apolakkia basin.

4. Inner forearc kinematics reflect simultaneous outward expansion of the Hellenic forearc, increasing curvature of the plate boundary, and associated boundary-parallel stretching of the forearc. Effects of sinistral-oblique plate convergence were not recorded in the Apolakkia basin but appear confined to the outer forearc and accretionary prism of the Mediterranean Ridge.

[53] **Acknowledgments.** Special thanks are due to Adriaan van Herk for his outstanding assistance in the field and many valuable discussions. This paper benefited from insightful conversations with Christian Teyssier and Basil Tikoff as well as discerning reviews by Hans Avé Lallement and Darrel Cowan. Dimitris Sakellariou kindly supplied critical background maps, and both IGME and the archeological survey of Rhodes provided the necessary fieldwork permits. This research was supported by National Science Foundation grant EAR-9815028.

References

Angelier, J., and P. Mechler, Sur une methode graphique de recherche des contraintes pricipales egalment utilisable en tectonique et en seismologie: La methode des diedres droits, *Bull. Soc. Geol. France*, *19*, 1309–1318, 1977.

Angelier, J., N. Lyberis, X. Le Pichon, E. Barrier, and P. Huchon, The tectonic development of the Hellenic arc and the Sea of Crete: A synthesis, *Tectonophysics*, *86*, 159–196, 1982.

Avé Lallemant, H. G., and L. R. Guth, Role of extensional tectonics in exhumation of eclogites and blueshists in an oblique subduction setting: Northern Venezuela, *Geology*, *18*, 950–953, 1990.

Avé Lallemant, H. G., and J. S. Oldow, Active displacement partitioning and arc-parallel extension of the Aleutian volcanic arc based on Global Positioning System geodesy and kinematic analysis, *Geology*, *28*, 739–742, 2000.

Benda, L., J. E. Meulenkamp, and W. J. Zachariasse, Biostratigraphic correlations in the eastern Mediterranean Neogene, 3, Correlation between mammal, sporomorph and marine microfossil assemblages from the upper Cenozoic of Rhodos, Greece, *Newsl. Stratigr.*, *6*, 117–130, 1977.

Besse, J., and V. Courtillot, Revised and synthetic apparent polar wander paths of the African, Eurasian, North American and Indian plates, and true polar wander since 200 Ma, *J. Geophys. Res*, *96*, 4029–4050, 1991.

Blair, T. C., and J. G. McPherson, Alluvial fans and their natural distinction from rivers based on morphology, hydraulic processes, sedimentary processes, and facies assemblages, *J. Sediment. Res.*, *64*, 450–489, 1994.

Bott, M. H. P., The mechanisms of oblique slip faulting, *Geol. Mag.*, *96*, 109–117, 1959.

Bruhn, R. L., and T. L. Pavlis, Late Cenozoic deformation in the Matanuska Valley, Alaska: Three-dimensional strain in a forearc region, *Geol. Soc. Am. Bull.*, *92*, 282–293, 1981.

Bukowski, G. V., Geologische Uebersichtkarte der insel Rhodus, *Jahrb. K. K. Geol. Reichsanst.*, *48*, 517–688, 1899.

Burbank, D., A. Meigs, and N. Brozovic, Interactions of growing fold and coeval depositional systems, *Basin Res.*, *8*, 199–223, 1996.

Cashman, S. M., H. M. Kelsey, C. F. Erdman, H. N. C. Cutten, and K. R. Berryman, Strain partitioning between structural domains in the forearc of the Hikurangi subduction zone, New Zealand, *Tectonics*, *11*, 242–257, 1992.

Célérier, B., Tectonic regime and slip orientation of reactivated faults, *Geophys. J. Int.*, *121*, 143–161, 1995.

Célérier, B., and M. Séranne, Breddin's graph for tectonic regimes, *J. Struct. Geol.*, *23*, 789–801, 2001.

Chanier, F., J. Ferriere, and J. Angelier, Extensional deformation across an active margin, relations with subsidence, uplift, and rotations: The Hikurangi subduction, New Zealand, *Tectonics*, *18*, 862–876, 1999.

Christie-Blick, N., and K. T. Biddle, Deformation and basin formation along strike-slip faults, in *Strike-Slip Deformation, Basin Formation, and Sedimentation*, edited by K. T. Biddle and N. Christie-Blick, *Spec. Publ. Soc. Econ. Paleontol. Mineral.*, *37*, 1–34, 1985.

Clifton, A. E., R. W. Schlische, M. O. Withjack, and R. V. Ackermann, Influence of rift obliquity on fault-population systematics: Results of experimental clay models, *J. Struct. Geol.*, *22*, 1491–1509, 2000.

Duermeijer, C. E., W. Krijgsman, C. G. Langereis, and J. H. ten Veen, Post-early Messinian counter-clockwise rotation on Crete: Implications for the late Miocene to Recent kinematics of the southern Hellenic Arc, *Tectonophysics*, *298*, 177–189, 1998.

Duermeijer, C. E., M. Nyst, P. T. Meijer, C. G. Langereis, and W. Spakman, Neogene evolution of the Aegean arc: Paleomagnetic and geodetic evidence for a rapid and young rotation phase, *Earth Planet. Sci. Lett.*, *176*, 509–525, 2000.

Duranti, D., Il "Levantino" fluvio-lacustre dell isola di Rodi (Grecia): Sedimentologia ed analisi di bacino, Ph.D. thesis, 110 pp., Univ. degli Studi Bologna, Bologna, 1997.

Fossen, H., and B. Tikoff, Extended models of transpression and transtension, and application to tectonic settings, in *Continental Transpressional and Transtensional Tectonics*, edited by R. E. Holdsworth, R. A. Strachan, and J. F. Dewey, *Geol. Soc. Spec. Publ.*, *135*, 15–33, 1998.

Fytikas, M., F. Innocenti, P. Manetti, R. Mazzuoli, A. Peccerillo, and L. Villari, Tertiary to Quaternary evolution of volcanism in the Aegean region, in *The Geological Evolution of the Eastern Mediterranean*, edited by J. E. Dixon and A. H. F. Robertson, *Geol. Soc. Spec. Publ.*, *17*, 687–699, 1984.

Gapais, D., P. R. Cobbold, O. Bourgeois, D. Rouby, and M. de Urreiztieta, Tectonic significance of fault-slip data, *J. Struct. Geol.*, *22*, 881–888, 2000.

Gautier, P., and J. P. Brun, Crustal-scale geometry and kinematics of late-orogenic extension in the central Aegean (Cyclades and Evvia Islands), *Tectonophysics*, *238*, 399–424, 1994.

Gawthorpe, R., I. Sharp, J. R. Underhill, and S. Gupta, Linked sequence stratigraphic and structural evolution of propagating normal faults, *Geology*, *25*, 795–798, 1997.

Geist, E. L., J. R. Childs, and D. W. Scholl, The origin of summit basins of the Aleutian Ridge: Implications for block rotations of an arc massif, *Tectonics*, *7*, 327–341, 1988.

Gupta, S., J. R. Underhill, I. R. Sharp, and R. L. Gawthorpe, Role of fault interactions in controlling synrift sediment dispersal patterns; Miocene, Abu Alaqa Group, Suez Rift, Sinai, Egypt, *Basin Res.*, *11*, 167–189, 1999.

Hanken, N., R. G. Bromley, and J. Miller, Plio-Pleistocene sedimentation in coastal grabens, north-east Rhodes, Greece, *Geol. J.*, *31*, 271–296, 1996.

Hansen, K. S., Development of a prograding carbonate wedge during sea level fall: Lower Pleistocene of Rhodes, Greece, *Sedimentology*, *46*, 559–576, 1999.

Harding, T. P., R. C. Vierbuchen, and N. Christie-Blick, Structural styles, plate tectonic settings, and hydrocarbon traps of divergent (transtensional) wrench faults, in *Strike-Slip Deformation, Basin Formation and Sedimentation*, edited by K. T. Biddle and N. Christie-Blick, *Spec. Publ. Soc. Econ. Paleontol. Mineral.*, *37*, 51–77, 1985.

Hardy, S., and J. Poblet, Geometric and numerical model of progressive limb rotation in detachment folds, *Geology*, *22*, 371–374, 1994.

Huchon, P., N. Lyberis, J. Angelier, X. Le Pichon, and V. Renard, Tectonics of the Hellenic Trench: A synthesis of Sea-Beam and submersible observations, *Tectonophysics*, *86*, 69–112, 1982.

Intergovernmental Oceanographic Commission—United Nations Educational, Scientific, and Cultural Organization (IOC-UNESCO), International bathy-

metric chart of the Mediterranean, scale 1:1,000,000, Paris, 1981.

Jolivet, L., A comparison of geodetic and finite strain pattern in the Aegean, geodynamic implications, *Earth Planet. Sci. Lett.*, *187*, 95–104, 2001.

Jongsma, D., Pliny and Strabo trenches, south of the Hellenic Arc, *Geol. Soc. Am. Bull.*, *88*, 797–805, 1977.

Kissel, C., and C. Laj, The Tertiary geodynamical evolution of the Aegean arc: A paleomagnetic reconstruction, *Tectonophysics*, *146*, 183–210, 1988.

Kovacs, E., and N. Spjeldnaes, Pliocene-Pleistocene stratigraphy of Rhodes, Greece, *Newsl. Stratigr.*, *37*, 191–208, 1999.

Leeder, M. R., and R. L. Gawthorpe, Sedimentary models for extensional tilt-block/half-graben basins, in *Continental Extensional Tectonics*, edited by M. P. Coward, J. F. Dewey, and P. L. Hancock, *Spec. Publ. Geol. Soc. London*, *28*, 139–152, 1987.

Le Pichon, X., Land-locked oceanic basins and continental collision: The Eastern Mediterranean as a case example, in *Mountain Building Processes*, edited by K. Hsü, pp. 201–211, Academic, San Diego, Calif., 1982.

Le Pichon, X., and J. Angelier, The Hellenic arc and trench system: A key to the neotectonic evolution of the eastern Mediterranean area, *Tectonophysics*, *60*, 1–42, 1979.

Le Pichon, X., et al., From subduction to transform motion: A Seabeam survey of the Hellenic trench system, *Earth Planet. Sci. Lett.*, *44*, 441–450, 1979.

Le Pichon, X., N. Chamon-Rooke, S. Lallemant, R. Noomen, and G. Veis, Geodetic determination of the kinematics of central Greece with respect to Europe: Implications for eastern Mediterranean tectonics, *J. Geoph. Res.*, *100*, 12,675–12,690, 1995.

Lourens, L. J., A. Antonarakou, F. J. Hilgen, A. A. M. van Hoof, C. Vergnaud-Grazzini, and W. J. Zachariasse, Evaluation of the Plio-Pleistocene astronomical timescale, *Paleoceanography*, *11*, 391–413, 1996.

Lowell, J. D., *Structural Styles in Petroleum Exploration*, 460 pp., Oil and Gas Consult. Int., Tulsa, Okla., 1985.

Marrett, R. A., and R. W. Allmendinger, Kinematic analysis of fault-slip data, *J. Struct. Geol.*, *12*, 973–986, 1990.

Mascle, J., A. Le Cleach, and D. Jongsma, The Eastern Hellenic margin from Crete to Rhodes: Example of progressive collision, *Mar. Geol.*, *73*, 145–168, 1986.

McCaffrey, R., Active tectonics of the eastern Sunda and Banda arcs, *J. Geophys. Res.*, *93*, 163–182, 1988.

McCaffrey, R., Estimates of modern arc-parallel strain rates in fore arcs, *Geology*, *24*, 27–30, 1996.

McClusky, S., Global Positioning System constraints on plate kinematics and dynamics in the eastern Mediterranean and Caucasus, *J. Geophys. Res.*, *105*, 5695–5719, 2000.

Meijer, P. T., and R. Wortel, Present-day dynamics of the Aegean region: A model analysis of the horizontal pattern of stress and deformation, *Tectonics*, *16*, 879–895, 1997.

Mercier, J. L., D. Sorel, and K. Simeakis, Changes in the state of stress in the overriding plate of a subduction zone: The Aegean Arc from the Pliocene to the present, *Annales Tectonicae*, *1*, 20–39, 1987.

Meulenkamp, J. E., E. F. J. de Mulder, and A. van de Weerd, Sedimentary history and paleogeography of the late Cenozoic of the island of Rhodos, *Z. Dtsch. Geol. Ges.*, *123*, 541–553, 1972.

Meulenkamp, J. E., M. J. R. Wortel, W. A. van Wamel, W. Spakman, and E. Hoogerduyn Straating, On the Hellenic subduction zone and the geodynamic evolution of Crete since the late middle Miocene, *Tectonophysics*, *146*, 203–215, 1988.

Mutti, E., G. Orombelli, and R. Pozzi, Geological studies on the Dodecanese islands (Aegean Sea), IX, Geological map of the island of Rhodes (Greece), explanatory notes, *Ann. Geol. Pays Hell.*, *22*, 77–226, 1970.

Peters, J. M., and W. H. Huson, The Pliny and Strabo trenches (eastern Mediterranean): Integration of seismic reflection data and SeaBeam bathymetric maps, *Mar. Geol.*, *64*, 1–17, 1985.

Petit, J. P., Criteria for the sense of movement on fault surfaces in brittle rocks, *J. Struct. Geol.*, *9*, 1243–1256, 1987.

Reches, Z., and J. H. Dieterich, Faulting of rocks in three-dimensional strain fields, I, Failure of rocks in polyaxial, servo-control experiments, *Tectonophysics*, *95*, 111–132, 1983.

Schlische, R. W., Geometry and origin of fault-related folds in extensional settings, *AAPG Bull.*, *71*(11), 1661–1678, 1995.

Smith, J. V., and D. W. Durney, Experimental formation of brittle structural assemblages in oblique divergence, *Tectonophysics*, *216*, 235–253, 1992.

Suppe, J., and D. A. Medwedeff, Geometry and kinematics of fault-propagation folding, *Eclogae Geol. Helv.*, *83*, 409–454, 1990.

Taymaz, T., J. Jackson, and D. McKenzie, Active tectonics of the north and central Aegean Sea, *Geophys. J. Int.*, *106*, 433–490, 1991.

Tchalenko, J. S., Similarities between shear zones of different magnitudes, *Geol. Soc. Am. Bull.*, *81*, 1625–1640, 1970.

ten Veen, J. H., and P. T. Meijer, Late Miocene to Recent tectonic evolution of Crete (Greece): Geological observations and model analysis, *Tectonophysics*, *298*, 191–208, 1998.

Teyssier, C., B. Tikoff, and M. Markley, Oblique plate motion and continental tectonics, *Geology*, *23*, 447–450, 1995.

Tron, V., and J. P. Brun, Experiments on oblique rift in brittle-ductile systems, *Tectonophysics*, *188*, 71–84, 1991.

van de Weerd, A., J. W. F. Reumer, and J. De Vos, Pliocene mammals from the Apolakkia Formation (Rhodes, Greece), *Proc. Kon. Ned. Ak. Wet., Ser. B*, *85*, 89–112, 1982.

van Vugt, N., Orbital forcing in late Neogene lacustrine basins form the Mediterranean, Ph.D. thesis, 167 pp., Utrecht Univ., Netherlands, 2000.

Walcott, C. R., and S. H. White, Constraints on the kinematics of post-orogenic extension imposed by stretching lineations in the Aegean region, *Tectonophysics*, *298*, 155–175, 1998.

Willmann, R., Die Alterstellung kontinentaler Neogenablagerungen in der Sudostlichen Agais (Rhodos und Kos/Dodekanes, Datca/Sudwestanatolien), *Newsl. Stratigr.*, *9*, 1–18, 1980.

Withjack, M. O., and W. R. Jamison, Deformation produced by oblique rifting, *Tectonophysics*, *126*, 99–124, 1986.

Woodside, J., J. Mascle, C. Huguen, and A. Volkonskaia, The Rhodes basin, a post-Miocene tectonic trough, *Mar. Geol.*, *165*, 1–12, 2000.

K. L. Kleinspehn, Department of Geology and Geophysics, University of Minnesota, Minneapolis, MN 55455, USA. (klein004@tc.umn.edu)

J. H. ten Veen, Department of Earth and Life Sciences, Free University, De Boelelaan 1085, 1081 HV Amsterdam, Netherlands. (veeh@geo.vu.nl)